The Pennsylvania State University
The Graduate School

SIMULATING METEOR BLAST WAVE PROPAGATION ON THE PLANET MARS USING NONLINEAR ACOUSTICS

A Thesis in
Acoustics
by
Lily Hetherington

Submitted in Partial Fulfillment
of the Requirements
for the Degree of

Master of Science

August 2024

The thesis of Lily Hetherington was reviewed and approved by the following:

Victor Sparrow
United Technologies Corporation Professor of Acoustics
Thesis Advisor

Amanda Hanford
Associate Research Professor of Acoustics

Christopher House
Professor of Geosciences

Andrew Barnard
Director of the Graduate Program in Acoustics

Abstract

Models of the Martian atmosphere from Bass and Chambers [2001], Williams [2001] and Petculescu [2016] predict that it absorbs sound more than Earth's atmosphere. The experiments that have been done with Ingenuity and are being done with the Perseverance microphone will begin to confirm the accuracy of such models [Maurice et al., 2022]. Because these models predict high sound absorption, even at short distances, only high amplitude, low frequency sound waves will propagate well on Mars. Meteors are an expected high amplitude sound source that have already been documented on Mars.

Presented is an analysis of simulation of the infrasound signature of a meteor blast wave as it would be received after traveling through the Martian atmosphere. Starting from replicating the absorption model from Bass and Chambers, a model of the Martian atmosphere that includes nonlinear behavior was built up to simulate high amplitude sound wave propagation. This work follows a similar approach that has been used to validate and update models used to predict meteor blast waves in the Earth's atmosphere [Edwards, 2009], [Nemec et al., 2017]. The augmented Burgers' solver developed by Cleveland and Hamilton was verified for nonlinearity and absorption that describe the Earth's atmosphere and then used to simulate these parameters for a model Martian atmosphere. A blast pulse for a meteor with a high Mach number is approximated as a cylindrical sound source that is propagated through a homogeneous form of the Martian atmosphere. The solver outputs the waveform as it would be received at a number of distances from the source.

Understanding meteor blast waves on Mars will help distinguish ground excitation by acoustic waves and meteorite impacts from seismic waves, improving study of Mars' seismology [Garcia et al., 2022]. In certain situations, these sounds might be heard by human visitors to Mars, so understanding the sounds will enhance astronaut safety and well-being.

The current model sets the stage for future validation efforts when measured data becomes available. In the future the model could be enhanced by utilizing a profile for an inhomogeneous model of the Martian atmosphere to use for the same simulations.

Table of Contents

List of Figures

List of Tables

List of Symbols

c	Sound speed
c_ν	Small signal sound speed increment
f	Frequency
f_r	Relaxation frequency
m	Dispersion parameter
p	Sound pressure
t_r	Relaxation time
v	Velocity
$\bar{x}$	Shock formation distance
C_p	Specific heat at constant pressure
C_v	Specific heat at constant volume
D	The ratio of atmospheric absorption to nonlinearity of a medium
α	Sound absorption coefficient
β	Coefficient of nonlinearity
γ	Ratio of specific heats
θ	Nondimensional relaxation time
κ	coefficient of thermal conductivity
μ_B	Bulk viscosity
ρ	Atmospheric density
σ	Nondimensional distance

τ Retarded time

ω Angular frequency

Acknowledgments

This work would not have been possible without the support of many people. I would like to start by thanking my advisor, Dr. Sparrow, for his shared curiosity in the worlds beyond our own, his guidance at every step of my research, and his encouragement to reach for every opportunity I could find. Next, I would like to thank Dr. Russell for his commitment to teaching, which provided funding for this research. I'd like to extended gratitude to Melissa Wandrisco and Lydia Olsen for always being in my corner, and keeping me on track for the aggressive deadlines I set for myself. I would like to thank all of my friends who have kept me honest, sane, and motivated but especially: Meg for encouraging all my best decisions, Kathryne for her endless faith in me, Wilder for being the best graduate student role model, and Chris for inspiring me. Finally, I would like to thank my family, for always seeing the best in me.

This work was supported, in part, by the United Technologies Corporation Professorship in Acoustics. I would like to acknowledge the University of Texas researchers who wrote and shared the code used in this work: Robin Cleveland, Mark Hamilton, and David Blackstock.

Chapter 1
Introduction

1.1 First Microhpone Sent to Mars

The Mars Polar Lander was the first Mars mission to include a microphone to take sound recordings on the red planet [NASA/JPL, 1999]. Although the mission failed, it sparked interest in the acoustics community to begin investigating how sound propagates on Mars. Since the mission, there have been papers published on models that predict the atmospheric absorption of sound, consideration of the characteristics of sound propagation from characteristic impedance to nonlinearity, and simulation of high frequency sound propagation in the Martian atmosphere. The work presented here aims to build on the theoretical research that has been conducted over the last 25 years. Recent and ongoing Mars missions have inspired this investigation of long range sound propagation of sonic booms.

1.2 Current Microphones on Mars

The Perseverance mission landed on Mars in February of 2021. Perseverance is a rover with the same type of microphone sent with the Mars Polar Lander built into the SuperCam instrument and a microphone built into the Ingenuity helicopter [Mimoun et al., 2023], [NASA/JPL, 2020]. Since the rover's landing, these microphones have provided recordings of a handful of sound sources: the environmental noise, laser induced spark sounds from Perseverance, and helicopter noise [Maurice et al., 2022]. A comparison of sound absorption models done by Maurice et al. is given in Figure 1.1 and shows an absorption coefficient for three octave bands that represent the frequencies of the laser source recorded by the Perseverance microphone. While they show there is

strong similarity in the absorption coefficient from the data to one one of the absorption coefficient models, more data in a larger frequency range is needed to get a clear picture of the sound absorption on Mars. During the continuation of the Perseverance mission, there will be opportunities for the SuperCam microphone to capture other sounds from Mars, a meteor being a plausible example. In the event of a meteor passing through the Martian atmosphere, recording the sound of the meteor and the meteorite impact is likely because they would be high amplitude sounds. A meteor would create a pulse wave that would have energy in a broadband frequency spectrum.

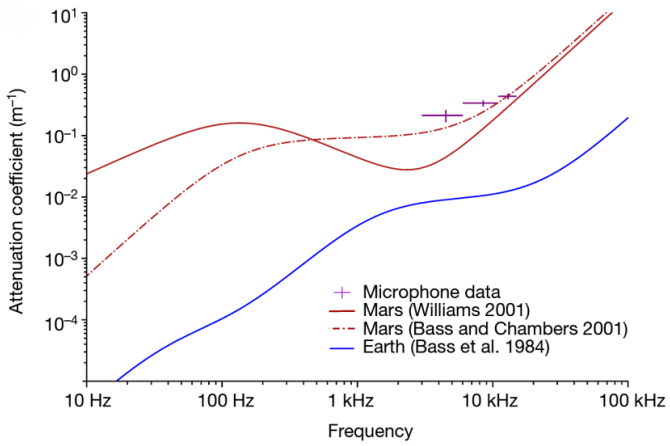

Figure 1.1: Comparison of two absorption coefficient models for Mars, the absorption coefficient model for Earth, and the absorption coefficients calculated for three octave bands from microphone data taken on Mars by the Perseverance rover [Maurice et al., 2022].

1.3 Other Acoustic Measurements

The InSight Lander was sent to Mars to study the interior of the planet[NASA, 2018]. The two main scientific goals were to gain an understanding of the formation and evolution of Mars, and to determine the level of tectonic activity of the planet. As is common for NASA missions, any opportunities to conduct other experiments were taken and Insight was used to study the atmosphere as well [Banfield et al., 2020]. Pressure sensors were among the data collection equipment on the InSight lander which allowed for detection of acoustic waves in the atmosphere from meteors. Using both the measured acoustic and seismic wave data, meteorite impact locations were estimated and later confirmed by imagery from the Reconnaissance orbiter [Garcia et al., 2022].

The Insight Lander was active on Mars for just over four years, and five impact events were confirmed from seismic and image data making a meteor event a likely sound source on the planet.

Being able to confirm seismic signatures of meteorite impacts allows for such activity to be separated from potential tectonic activity of the planet. Having microphones on Mars that could capture acoustic data from meteors would add more confidence to determining seismic activity from meteoroid impacts versus tectonic activity. This work presents a prediction of the propagation of a sonic boom from a meteor traveling through the Martian atmosphere. To do so, we create an model of the Martian atmosphere, and a model of a meteor blast wave to propagate through the modeled atmosphere.

1.4 Meteor Blast Waves

Meteors travel at speeds has high as Mach 74 in the Martian atmosphere, which is about Mach 58 on Earth [Edwards, 2009]. For reference, super sonic aircraft travel at Mach speeds in the single digits. With sounds sources traveling above the speed of sound, assumptions that are made to use a linear wave equation are no longer valid. One form of nonlinear behavior of high amplitude sound is energy that in linear behavior would be attenuated, is cycled into the higher frequency content of the wave. The energy going to the higher frequencies allows the high amplitude wave to propagate longer distances than a wave that behaves linearly. One of the simplest nonlinear wave equations known as the Burgers equation, is used in this work to model the propagation of a meteor blast in both Earth's atmosphere and the Martian atmosphere.

Meteor-generated blast waves have not yet been recorded on Mars. In order to create a realistic blast pulse from one for the Martian atmosphere, models of meteor behavior in Earth's atmosphere were considered. Due to the implementation of the International Monitoring System (IMS), there have been a number of meteor events recorded as infrasound propagation through Earth's atmosphere. Analytical models have been made and improved upon throughout the years as more data from the IMS has been analyzed [Edwards, 2009]. In the model, a meteor Mach cone is approximated as a cylindrical sound source and nonlinear weak shock theory is used as shown in Figure 1.2.

In more recent years, numerical models have been used to simulate what the blast pulse near the cylindrical meteor source might look like, including how much the pressure might jump from the ambient pressure [Henneton et al., 2015], [Nemec et al., 2017].

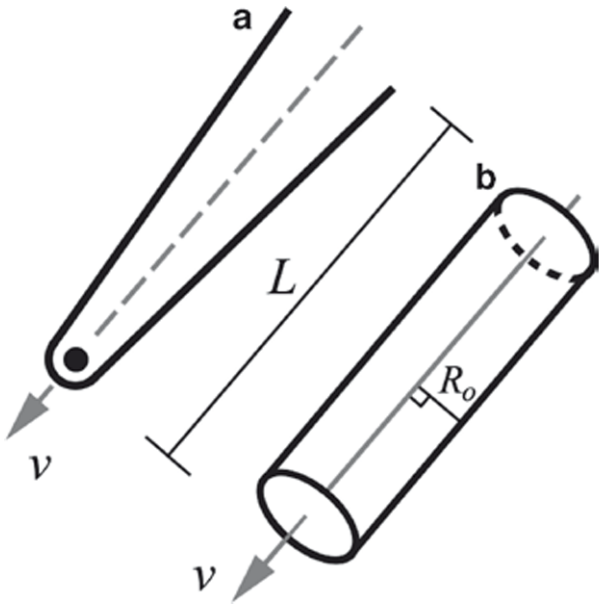

Figure 1.2: a) A diagram of a meteor Mach cone and b) the approximation of the meteor Mach cone as a cylindrical line source with radius R_0 and length L [Edwards, 2009].

Complex fluid dynamic computation was used in both of the referred models to predict the behavior and amplitude of the initial blast pulse. Shown in Figure 1.3 is an example of one of the blast pulses produced by Nemec et al. to propagate through a numerical Burgers' solver to compare to data collected from the IMS. The pressure axis is scaled by the ambient pressure, p_∞, where Δp is the change in pressure from ambient due to the meteor. For shocks from supersonic movement, the waveform is expected to have both a front and back shock. While this is commonly seen with aircraft, a meteor's speed is so fast, the waveform resembles an explosion blast wave.

1.5 Overview

The purpose of this thesis is to present a model of high amplitude sound propagation in the Martian atmosphere to show that nonlinear acoustic theory used for Earth applies to Mars and can be used as tool in future missions to Mars. The model is built up from the most simplified case of sound propagation in an atmosphere by adding realistic complex properties one at a time and examining how each affects the sound propagation. To start, the sound speed, impedance, and velocity and pressure relationship are defined for Mars and compared to Earth. Sound absorption by the atmosphere is added next

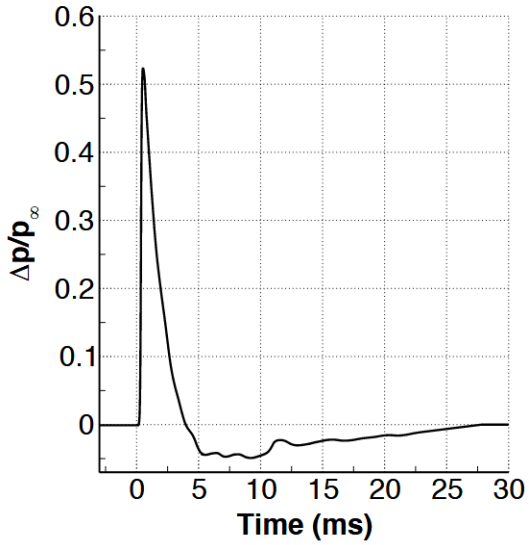

Figure 1.3: Nearfield blast pulse prediction for Meteor 20090428 in Earth's atmosphere Nemec et al., 2017

and analyzed for plane wave propagation as there are no other attenuation effects that have to be considered. The analysis of these properties shows that sounds on Mars are quieter and only travel short distances. Nonlinear acoustics is investigated next because signals that behave in a nonlinear manner on Earth travel greater distances than linear signals. An analytical solution of the Burgers Equation is found using parameters of the Martian atmosphere. This allows for a preliminary analysis of the nonlinearity of the Martian atmosphere in comparison to the effect of sound absorption. Finally, a numerical method is used to predict high amplitude wave propagation in an atmospheric model that includes nonlinearity and molecular relaxation to show that a high amplitude signal should propagate long distances. This is despite having a lower peak pressure than the same signal would have on Earth and the high absorption by the atmosphere on Mars.

Chapter 2
Characteristics of Mars

2.1 The Martian Atmosphere and Simplifications

Mars has an atmosphere the differs greatly from Earth, which drives the differences in sound propagation. It has an ambient pressure at the surface of 6.36 mb (636 Pa) with a range from 4 to 8.7 mb depending on the season. The surface density of the atmosphere is roughly 0.020 kg/m^3. The major composition consists of 95.1% carbon dioxide, 2.59% nitrogen, 1.94% argon, and 0.016% oxygen, with trace amounts of water vapor [NASA, 2024]. This information is shown in Figure 2.1. For this work, the contributions of the water vapor were not considered. The temperature range and sound speed used were based on the same values used by Bass and Chambers in their model for atmospheric absorption on Mars [2001]. This was the model used for absorption in this work. Bass and Chambers calculated absorption coefficients for 200 K and 300 K, and values from the 300 K case were used for comparison to a typical temperature on Earth of 293 K. At 300 K the equilibrium sound speed on Mars is calculated to be 273.4 m/s using the following equation,

$$c = \sqrt{\gamma RT/M} \tag{2.1}$$

where γ is the ratio of specific heats, R is the gas constant in J(kmol)$^{-1}$K^{-1}, and M is the molecular weight in kg (kmol)$^{-1}$.

Simplifications of the atmosphere were made to make all calculations feasible and timely. The atmosphere was considered homogeneous, meaning it does not change in density nor pressure for the propagation distances used. For both analytical and numerical solutions, a sonic boom from a meteor was considered at near surface altitude, received as a horizontal and one-dimensional propagation. The pressure and density of

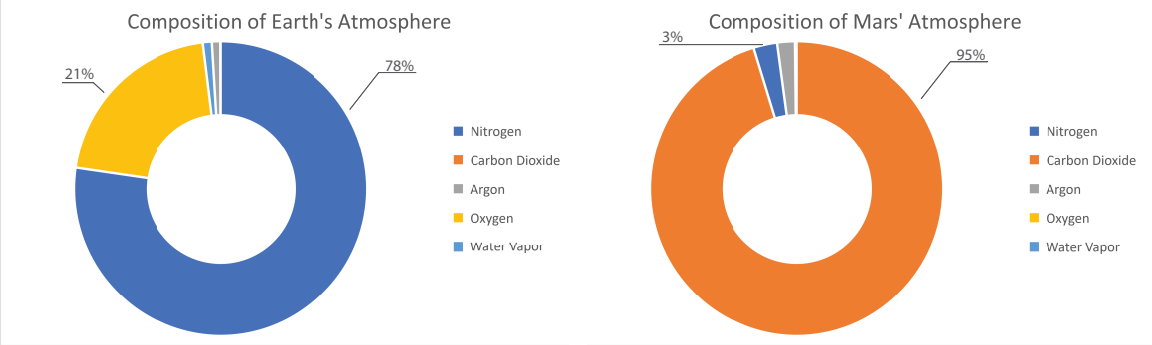

Figure 2.1: Comparison of the gaseous mixtures of Earth and Mars' atmospheres. Earth is predominately nitrogen and oxygen gas. Mars is predominately carbon dioxide.

the atmosphere are representative of an altitude near the planet's surface, the analysis was done as for a free field, without any reflections. A sonic boom from a meteor is the sound source considered in this work.

In previous work done to study acoustics on Mars, the atmosphere was modeled directly as particles to simulate their motion and collisions because it is valid for all Knudsen numbers [Hanford and Long, 2009]. The Knudsen number is defined as the ratio of the mean free path to the length scale of the system being modeled. This is necessary for high frequency signals and dilute gases where the continuum theory breaks down. The continuum theory works on the assumption that the media being modeled entirely fills the space it occupies. This assumption becomes problematic for the higher altitudes of atmospheres and for frequencies that have wavelength at or smaller than the length scale of the system. The system being considered for this work is for very low Knudsen numbers (large wavelengths) making use of continuum theory valid.

The next section discusses how the density, temperature, and pressure of the Martian atmosphere affect sound propagation. The pressure amplitude of a plane sound wave is affected by the characteristic acoustic impedance of the atmosphere.

2.2 Impedance in the Atmosphere

Impedance in acoustics is defined as the pressure divided by velocity, which can be volume or particle velocity. For a plane wave the ratio between pressure and particle velocity equals the density of the medium times the sound speed in that medium. This is called the characteristic impedance, z and takes the form

$$z = \rho c \tag{2.2}$$

The density and sound speed are dependent only on the properties of the medium, so the characteristic impedance describes how well the medium responds to pressure fluctuations. The characteristic impedance of Earth's atmosphere at sea level and ambient temperature is 415.03 rayls, and the characteristic impedance of Mars' atmosphere with the density and sound speed described in the previous section is 5.468 rayls. The density of the Earths atmosphere is significantly larger than that of Mars, making the characteristic impedance for Mars about 1% of Earth's.

To think of the effect this has on a real system, it can be helpful to use specific radiation impedance. Specific radiation impedance relates the pressure a mechanical system has to the particle velocity it creates in a medium. The real part of radiation impedance ($Re\{Z_{rad}\}$) is the energy being removed from the system, in this case it is the power radiated as sound [Pierce, 1981, Sec 3.5, Eq. (3.5.11)]. $Re\{Z_{rad}\}$ is proportional to the characteristic impedance, so the sound power a mechanical system radiates on Earth would be reduced by a factor of 100 on Mars. This is a 20 dB reduction in sound pressure level [Sparrow, 1999]. For example, vibrating machinery such as an air handling unit on a building, could have a sound pressure level on Earth near 80 dB. The same equipment would have a sound pressure level of 60 dB on Mars while working in the same manner. Psychoacoustics points out that a 10 dB drop in sound level is perceived by most people as being half as loud, making a 20 dB drop in sound level correspond to a perception of a sound being a quarter as loud [Begault, 1994]. Sounds on Mars are about a quarter as loud as sounds on Earth.

2.2.1 Velocity and Pressure

For Earth and Mars, the relationship of acoustic pressure and velocity of a plane wave stays the same, the velocity is related to the pressure by the characteristic impedance

$$v = \frac{p_E}{\rho_E c_E} = \frac{p_M}{\rho_M c_M} \tag{2.3}$$

where the subscripts denote for Earth and for Mars. A vibrating source on both planets has the same power supply and would create the same velocity in each atmosphere with the force it exerts. Because the characteristic impedance on Mars is smaller, the pressure on Mars must also be smaller in order for the velocity to stay the same. A blast pulse from a meteor will have the same reduced pressure amplitude. In Chapter 5, a meteor

event recorded on Earth with the pressure scaled by the characteristic impedance of Mars is used as basis to create an appropriate initial blast pulse to propagate through a model of the Martian atmosphere.

2.3 Summary

A lot can be determined about sound propagation on Mars from looking at the simplest case: a plane wave traveling through the open atmosphere, ignoring attenuation, wind, and nonlinear acoustics. Due to the low temperatures and very low density of the Martian atmosphere, any kind of sounds will have a 20 dB lower sound pressure level than they would have on Earth. Sounds on Mars start off quieter than on Earth, and it will be shown in the next chapter, that higher frequencies are quickly attenuated by the atmosphere as well.

Chapter 3
Sound Absorption on Mars

3.1 Current Models

The absorption of sound in the atmosphere is a defining characteristic of sound propagation on Mars, with all models predicting that sound will be attenuated more severely on Mars than it is on Earth. Petculescu and Lueptow [2007] used an eigenvalue method to solve for an effective wavenumber, from which an absorption coefficient can be backed out. This model was not used for the work presented, but it is noted that the results agree with the Bass and Chambers model.

Williams published an overview of acoustics on Mars [2001] to discuss what work could have been done in the field, if the Mars Polar Lander had been a successful mission. As part of this overview, they derived a model for the sound absorption. This model used experimental data for the thermal relaxation of carbon dioxide in Earth's atmosphere to derive an equation for the relaxation absorption on Mars as well as a different formulation for the viscous absorption coefficient. It differs greatly from the models for all frequencies, and predicts a higher absorption overall than the other models. Figure 3.1 shows a comparison of the three absorption models versus frequency.

The absorption model that was verified and used for this work is from Bass and Chambers [2001]. It was chosen because it follows the same process that is used by Bass et al. for the model of sound absorption on Earth for lower altitudes and it has the closest match to the preliminary data from the Perseverance mission, shown earlier in Figure 1.1 [Maurice et al., 2022].

This section will discuss the methods used to replicate the results of the Bass and Chambers model. The thermovicous absorption equation is defined. Absorption from both vibrational and rotational relaxation are considered separately. All three forms of absorption are compared to evaluate which type has the greatest effect on the overall

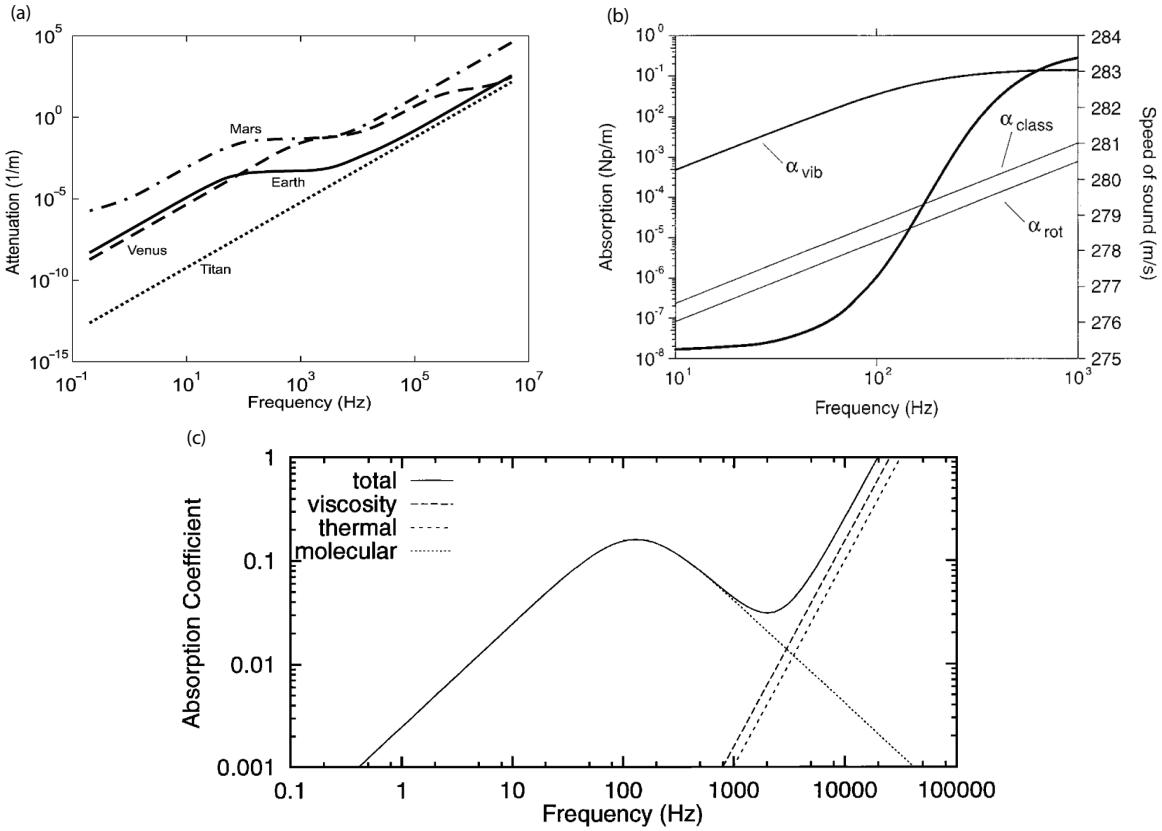

Figure 3.1: Plots of absorption coefficient versus frequency from (a) Petculsescu and Lueptow [2007], showing total sound absorption for Mars (b) Bass and Chambers [2001] showing the vibrational relaxation absorption, rotational relaxation absorption, and the classical absorption (for a temperature $T = 300$ K), and (c) Williams [2001] showing absorption for thermal, molecular, and viscous absorption as well as the sum of the three.

sound absorption. The absorption coefficient for two low frequencies are used from this model to visualize the propagation of a sinusoidal plane wave in the Martian atmosphere.

3.2 Calculation of Absorption

The model of sound absorption by a fluid used in this work for both Mars and Earth considers absorption from thermoviscous properties and the relaxation processes of the components of the fluid. For Earth, this is the vibrational relaxation processes of nitrogen and oxygen. For Mars, thermoviscous absorption, virbational and rotational relaxation of carbon dioxide are compared to discern which process has the greatest effects over a range of frequencies from infrasound to the audible range. The equation for classical absorption (also referred to as the thermoviscous absorption) remains the same for Earth and Mars. The atmosphere of Mars can be considered an ideal gas, so use of this method is valid. There are a few formulations of the classical absorption and the following equation was used for the absorption coefficient α:

$$\alpha_{cl} = [\omega^2/(2\rho^0 c^3)][4\mu/3 + (\gamma - 1)\kappa/(\gamma C_v)] \tag{3.1}$$

where ω is the angular frequency, ρ_0 is the equilibrium density in kg/m^3, c is is the speed of sound in m/s, μ is the coefficient of viscosity in kg/m, γ is the ratio of specific heats, κ is the coefficient of thermal conductivity in J(kg kmol)$^{-1}$K^{-1}kg m^{-1} s^{-1}, and C_v is the specific heat at constant volume in J(kg kmol)$^{-1}$K^{-1} [Bass and Chambers, 2001].

The molecular relaxation of carbon dioxide was the only relaxation process considered for the calculation because it makes up 95% of the atmosphere of Mars. The equation for the absorption coefficient from rotational relaxation is

$$\alpha_{rot} = [2\pi^2 f^2/(\gamma P c)]\mu[\gamma(\gamma - 1)R/(1.25C_P^0)]Z_{rot} \tag{3.2}$$

where P is the atmospheric pressure, f is the frequency in hertz, c is the sound speed calculated with a ratio of specific heats that excludes the vibrational contribution, R is the gas constant, C_P^0 is the specific heat at a constant pressure for a frequency that is above the relaxation frequency for vibration, and Z_{rot} is the rotational collision number for carbon dioxide. A collision number is the rate of collisions between two molecule in a volume, and the rotational collision number depends upon the rotational energy spacing. It was assumed that the rotational collision number for carbon dioxide, oxygen, and nitrogen would be very similar and the equation for Z_{rot} was based off of measurements for oxygen and nitrogen [Bass and Chambers, 2001].

$$Z_{rot} = 61.1 \exp(-16.8/T^{1/3}) \tag{3.3}$$

The equation used to calculate the absorption from vibrational relaxation is

$$\alpha_{vib} = (\pi s/c)(f^2/f_r)/[1 + (f/f_r)^2] \tag{3.4}$$

where s is the relaxation strength, and f_r is the relaxation frequency. The relaxation strength compares the specific heat at constant volume for each molecular species to the specific heat at constant pressure and volume well above the relaxation frequency for carbon dioxide. The relaxation frequency is the reciprocal of the relaxation time, t_r, which is the time it takes for the molecule to return to equilibrium. The relaxation time is found by calculating the rate at which the doubly degenerate bending mode of carbon dioxide will transfer vibrational energy to other molecules in the atmosphere, denoted as k. For Mars, Bass and Chambers considered collisions with carbon dioxide (CO_2), nitrogen (N_2), argon (Ar), and water vapor (H_2O). The total forward rate is the sum of the rate of transfer to each type molecule multiplied by the mole fraction for each type of molecule. The difference in the forward rate of the reaction, k, and the reverse rate of the reaction, k_b, is the inverse of the relaxation time at a constant volume and temperature. To get the relaxation time for a single energy transfer, the relaxation time at constant volume and temperature is multiplied by a ratio of the specific heat at constant pressure for frequencies well above the relaxation frequency to the specific heat at constant pressure for frequencies far below the relaxation frequency.

Vibrational and rotational relaxation processes were calculated and compared with the classical absorption. The comparison shows that vibrational relaxation of carbon dioxide molecules are responsible for most of the atmospheric absorption for frequencies below 10^3 in magnitude. Figure 3.2 shows that the absorption is considerably lower for low frequencies. In the next section, the effect of the absorption on Mars is compared to the effect on Earth.

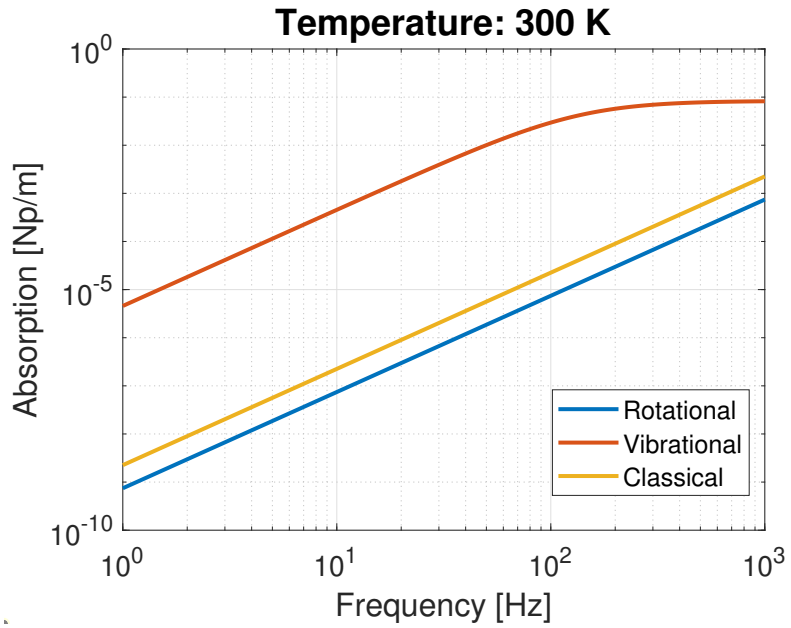

Figure 3.2: Sound absorption coefficient by the atmosphere as a function of frequency from classical absorption, rotational and vibrational relaxation of carbon dioxide.

3.3 Comparison to Earth

To visualize the difference of absorption from Earth to Mars, a simple model of a plane wave source was made in each atmosphere. A plane wave has no attenuation from spreading, and shows only the effect of the atmospheric absorption on the sound level as the receiver gets further away from the source. The source has a sound pressure level (SPL) of 90 dB. The SPL per distance from sources with two different frequencies are shown in Figure 3.3 and Figure 3.4. For a source emitting a 100 Hz plane wave, there is no change in sound level on Earth at 400 meters distance from the source, whereas on Mars the sound can no longer be heard. For a source that emits a 10 Hz frequency, the absorption is much lower and it can be seen that for both Earth and Mars, the signal travels significantly farther. For this reason, infrasound was chosen as the region of sound to focus on when studying sound propagation on Mars. A shock wave from a meteor will produce sound in all frequencies, and it is plausible that the lower frequency content could reach a microphone hundreds to thousands of meters away.

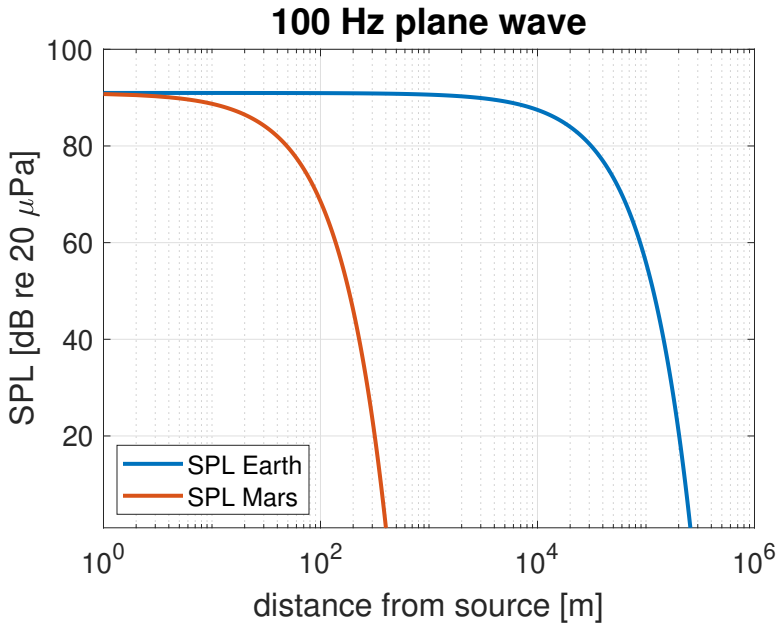

Figure 3.3: Comparison of the sound pressure level (SPL) as a function of distance for a source producing a 100 Hz plane wave in Earth's atmosphere and Mars' atmosphere.

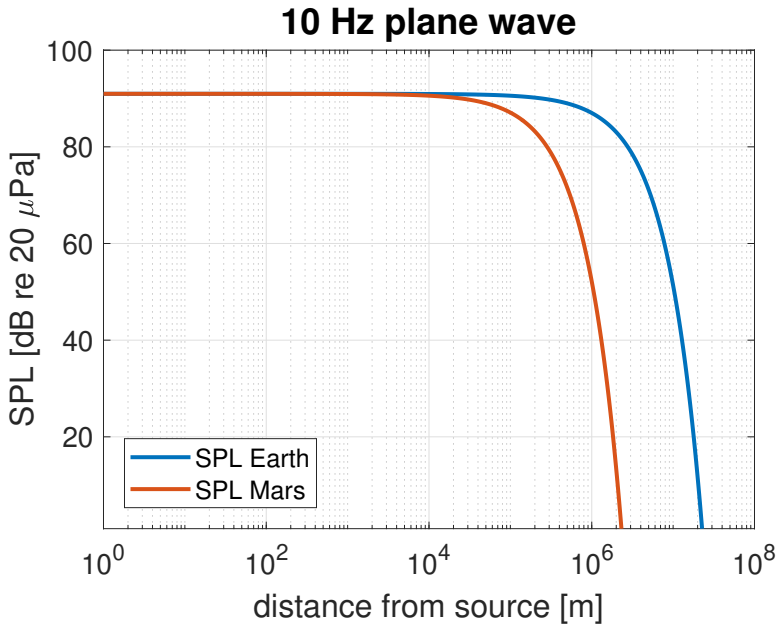

Figure 3.4: Comparison of the sound pressure level (SPL) as a function of distance for a source producing a 10 Hz plane wave in Earth's atmosphere and Mars' atmosphere.

3.4 Summary

In order to understand the sound propagation in any media, the properties of the media must first be well defined. For acoustics in fluid media, the absorption of sound by

the fluid is a critical parameter for sound propagation. For highly absorbing fluids, like the Martian atmosphere, if the absorption is not properly calculated, experimental setups could be affected because the sound might not reach the receiver. As daily observers of atmospheric acoustics on Earth, it is easy to make assumptions based on experience. The comparison of the SPL of a sinusoidal source in each atmosphere provides a more intuitive visualization of the sound absorption on Mars and confirms that only low frequency sound waves will travel long distances on Mars. A source such as a sonic boom from a meteor emits a large amount of energy in the low frequency part of the spectrum. With high amplitude sound sources, linear acoustics does not accurately predict the behaviour of the sound. The next section will discuss the nonlinearity of the Martian atmosphere, which is integral to modeling sonic boom propagation.

Chapter 4
Burgers' Equation: Analytical Solution

For high amplitude sounds, the assumption of linearity of the wave equation is no longer valid, and certain nonlinearities must be considered to accurately calculate the pressure and velocity of such sounds. This chapter focuses on the the formulation of the wave equation known as the Burgers Equation which has solutions that can be found analytically. Using the properties of the Martian atmosphere in this calculation provides a preliminary look at whether the behavior of a meteor blast wave on Mars would be the same as expected on Earth.

4.1 The Burgers Equation

The Burgers Equation is used for comparing the effects of nonlinearity and dissipation. It is the simplest form of a nonlinear wave equation and can be solved without numerical methods for certain situations such as the case of an initially sinusoidal wave.

$$\frac{\partial p}{\partial x} - \frac{\delta}{2c_0^3}\frac{\partial^2 p}{\partial \tau^2} = \frac{\beta p}{\rho_0 c_0^3}\frac{\partial p}{\partial \tau} \tag{4.1}$$

It describes the pressure changes over space and time with x for distance, p for pressure, and τ for retarded time. Retarded time is defined as $\tau = t - x/c_0$, the difference in a moment in time and the time it takes for the sound to travel to the point in space at that time. The affects of thermoviscous absorption are included as a dissipation coefficient

$$\delta = \rho_0^{-1}[\frac{4}{3}\mu + \mu_B + \kappa(C_v^{-1} - C_p^{-1})] \tag{4.2}$$

where μ is the shear viscosity, μ_B is the bulk viscosity, κ is thermal conductivity.

The right hand side of equation 4.1 is the nonlinear component, and β is the coefficient of nonlinearity. As previously mentioned, the Maritain atmosphere can be considered an ideal gas, which allows β to be defined as

$$\beta = \frac{(\gamma + 1)}{2} \tag{4.3}$$

Because of the importance of the molecular relaxation of carbon dioxide to the sound absorption on Mars, a more complex form of the Burgers Equation that include the affects of the molecular relaxation processes is needed. For this step of modeling the Martian atmosphere, it is assumed that it is entirely carbon dioxide which allows for the molecular relaxation to be considered while solving the simpler form of the Burgers Equation given in Equation 4.1. The thermoviscous absorption is significantly smaller than the relaxation absorption from carbon dioxide so the dissipation from thermoviscous absorption was considered negligible for this model.

4.2 Monorelaxing Fluid

Assuming that the Martian atmosphere is only carbon dioxide, it can be modeled as a monorelaxing fluid in order to solve for the solution of the Burgers Equation directly. The example of a monorelaxing fluid presented in the Hamilton and Blackstock book on nonlinear acoustics was used as a comparison for this model [1998]. They introduce an important parameter, D, which is defined as the ratio of relaxation effects to nonlinear effects,

$$D = \frac{m\rho_0 c_0^2}{2\beta p_0} \tag{4.4}$$

where m is the dispersion parameter, ρ_0 is the ambient density of the atmosphere, c_0 is the equilibrium sound speed, β is the coefficient of nonlinearity, and p_0 is the initial peak amplitude of the shock. The ratio is a quick way to determine whether the effects of nonlinearity or absorption will be dominant in shaping the waveform. When $D > 1$, absorption is dominating nonlinearity and the wavefront with have a longer rise time and shock thickness. The wavefront has a smooth behavior when it reaches the peak negative and positive pressures. When $D = 1$, absorption and nonlinearity are equally affecting the shock. The rise time and shock thickness are shorter, but a discontinuity jump has not appeared yet. Once $D < 1$, the nonlinearity begins to dominate absorption and a discontinuity appears because the pressure wave cannot be multi-valued. This behavior

is shown in the results section of this chapter.

The dispersion parameter, m, is the square difference between the frozen speed (the sound speed at high frequencies), c_∞, and equilibrium sound speed (the sound speed at low frequencies), c_0, relative to the square of the equilibrium sound speed. It is an indicator of how influential the molecular relaxation process is to the absorption of sound by considering how large the dispersion is.

$$m = (c_\infty^2 - c_0^2)/c_0^2 \tag{4.5}$$

The only value of D that changes with time or space in a homogeneous atmosphere is the peak pressure amplitude of the shock wave. For an atmosphere that has higher dispersion, only large shocks will have a D value greater than 1. Table 4.1 shows pressure amplitude values and their corresponding ratio of absorption to nonlinearity for carbon dioxide under the conditions of the Martian environment.

Table 4.1: The relationship of acoustic pressure amplitude and the ratio of relaxation effects to nonlinear effects (D) of the Martian atmosphere; as described as a monorelaxing fluid.

Pressure [Pa]	D
1	50.45
2	25.22
5	10.10
20	2.52
50	1.00
100	0.51

In Chapter 5 of Nonlinear Acoustics [Hamilton and Blackstock, 1998], they present waveforms in a non-specified monorelaxing fluid for values of $D = 2$, $D = 1$, and $D = 0.5$. Once the nonlinearity of the fluid starts to out compete with absorption ($D < 1$), the solution to the Burgers Equation will become multivalued, or have two values for pressure, for some values of τ. This is not physically possible, and a mathematical correction known as weak shock theory is used to evaluate the Burgers Equation near the shock. Weak shock theory is used to find the pressures just before, and just after the shock which determines the final waveform. The solution to the Burgers Equation given by Hamiliton and Blackstock is

$$\tau = t_r \ln \frac{(1 + p/p_0)^{D-1}}{(1 - p/p_0)^{D+1}} \tag{4.6}$$

where τ is retarded time, t_r is the relaxation time of the monorelaxing fluid, p is the pressure of the waveform at any point, and p_0 is the peak pressure amplitude. For $D \gg 1$, Equation 4.6 can be rearranged to have pressure as a function of retarded time,

$$p = p_0 \tanh(\tau/2Dt_r) \tag{4.7}$$

For $D = 1$ Equation 4.6 simplifies to

$$p = p_0[1 - \exp(-\tau/2t_r)] \tag{4.8}$$

When $D \leq 1$, Equation 4.6 is evaluated using weak shock theory. For a shock modeled as an instantaneous pressure jump, the sound speed just before and after the jump is

$$c_\infty = (1 + m/2)c_0 \tag{4.9}$$

and the shock must propagate with a speed of

$$\frac{dx_{sh}}{dt} = c_\infty + \beta(p_{sh} - p_0)/2\rho_0 c_0 \tag{4.10}$$

The shock is stationary in the retarded time frame meaning that $\frac{dx_{sh}}{dt} = c_o$. When setting these equations equal to each other, they can be rearranged to get an expression for the pressure of the shock, p_{sh} [Hamilton and Blackstock, 1998].

$$p_{sh} = (1 - 2D)p_0, 0 \leq D \leq 1 \tag{4.11}$$

The pressure at the shock is used in Equation 4.6 to calculate the point in time, τ_{sh}, of the discontinuity.

$$\tau_{sh} = -t_r \ln[4D^{1+D}(1 - D)^{1-D}] \tag{4.12}$$

Before the arrival time of the shock, pressure is equal to the negative peak pressure, and at the arrival time and after, it is described by Equation 4.6. To evaluate Equation 4.6 for pressure, a solver for the zeros of nonlinear equations was used. More detail on this process is given in Appendix B. The next section discusses the results of this process in the context of Mars.

4.3 Results

The values of D chosen for evaluation were 2.5, 1, and 0.5 to compare to the example from Hamilton and Blackstock and were first presented at the 184th conference of the Acoustical Society of America [Hetherington and Sparrow, 2023]. The peak pressure amplitudes corresponding to these values are possibly larger than would be realistic on Mars; the next chapter includes consideration of what a realistic pressure value would be for a meteor blast on Mars.

The rise time and shock thickness of each wavefront are show in Table 4.2. The rise time used here is the time it takes for the pressure to rise from 10% of the shock jump pressure to 90% of the shock jump pressure. The shock thickness is the distance in space of the shock. As D decreases, both the shock thickness and rise time decrease. The peak amplitude is increasing, so a louder shock has a smaller rise time and a smaller thickness. This behavior is seen in Table 4.2 for D values calculated with the sound speed and density of the Martian atmosphere.

Table 4.2: The rise time and shock thickness of the initial rise of a blast in the Martian atmosphere as a function of D.

D	Rise time [s]	Shock thickness [m]
2.5	0.081	22.1491
1	0.033	9.0237
0.5	0.018	4.9220

Figures 4.1, 4.2, and 4.3 show the change in wavefront behavior as D decreases. When $D = 2.5$, a shock has not yet formed as there is a smooth transition from negative to positive peak pressure, and a longer rise time. The energy of the shock is spread out over time and space by the absorption of the atmosphere. When $D = 1$, both nonlinearity and absorption affect the behavior. A pressure jump has not yet occurred, but the transition from the negative pressure in no longer smooth. The asymmetric behavior is a result of the molecular relaxation. For $D = 0.5$, the nonlinearity dominates and there is an obvious jump in pressure. The vertical jump is a result of the analytical solution. Using a numerical solver would have more resolution near the shock itself. Figure 2 from Chapter 5 of Hamilton and Blackstock's book has both a normalized pressure axis and time axis, but the behavior of each wavefront is comparable. With the agreement of these results to the example of a shock in a monorelaxing fluid from Hamilton and Blackstock, it is reasonable to continue with nonlinear acoustic theory to build a more accurate model of a shock wave in the Martian atmosphere.

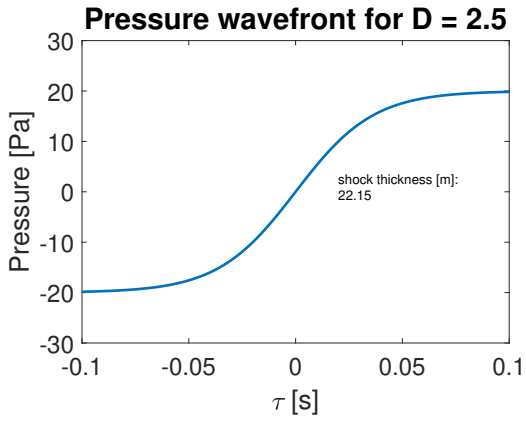

Figure 4.1: Pressure wavefront for $D = 2.5$, no shock has formed.

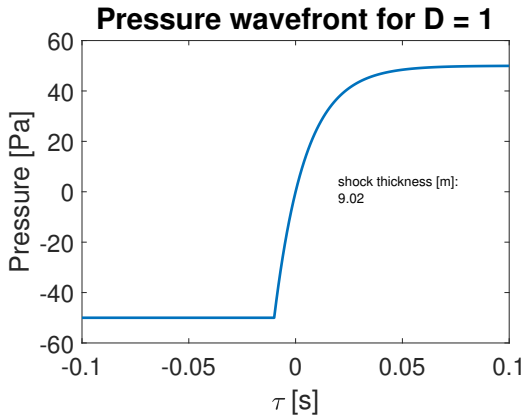

Figure 4.2: Pressure wavefront for $D = 1$, a slope discontinuity has formed but the pressure is not yet multivalued.

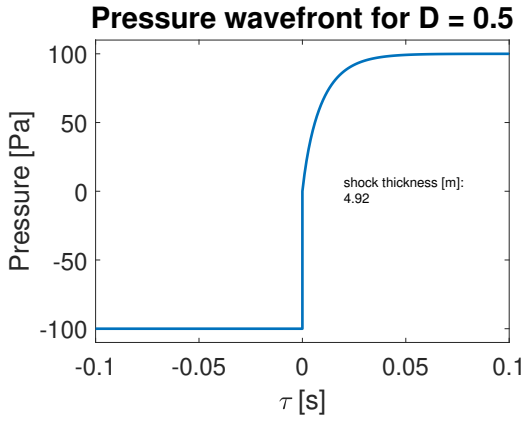

Figure 4.3: Pressure wavefront for $D = 0.5$, which would be multivalued without using weak shock theory.

4.4 Summary

When the Martian atmosphere is modeled as a homogeneous monorelaxing fluid made up entirely of carbon dioxide, there is good reason to believe that shock waves will propagate through it in an expected way. The wavefronts calculated match the comparison with a general monorelaxing fluid. By confirming that nonlinear acoustic theory should work for the Martian atmosphere, a numerical method can be employed to create a more accurate model of shock wave propagation. The next chapter discusses the augmented Burgers Equation and the numerical methods used to solve it and simulate wave propagation for an actual meteor blast.

Chapter 5
Burgers' Equation: Numerical Solution

Modeling the Martian atmosphere using the Burgers Equation allows for fast calculation, but is not necessarily realistic because it oversimplifies the atmosphere by excluding many of its properties. Using numerical methods to solve an augmented form of the Burgers Equation can confirm how accurate the analytical solution is, and allows for complexities of an atmosphere to be included in the model. This chapter describes the augmented Burgers Equation, the solver used to compute wave propagation, model a realistic meteor blast wave, and compare to other acoustic models for wave propagation.

5.1 Augmented Burgers' Equation

The form of the Burgers Equation used for the rest of this work is taken from Cleveland et al. which they derived from Pierce [1981].

$$\frac{\partial p}{\partial x} - \frac{\delta}{2c_0^3}\frac{\partial^2 p}{\partial \tau^2} = \frac{\beta p}{\rho_0 c_0^3}\frac{\partial p}{\partial \tau} + \sum_\nu \frac{c'_\nu}{c_0^2}\int_{-\infty}^{\tau} \frac{\partial^2 p}{\partial t''^2} e^{-(\tau - t'')/t_\nu} dt'' \tag{5.1}$$

The formulation is the same as the Burgers Equation from Chapter 4 with the addition of a sum that takes into account the effects of molecular relaxation. The sum allows for ν number of relaxation processes, with c'_ν being a small-signal sound speed increment, t_ν is the relaxation time, and t'' a place holder variable for integration. The small-signal sound speed increment is the change in sound speed with frequency due to the relaxation processes in an atmosphere. This change in sound speed with the change in frequency is known as dispersion. In the Earth's atmosphere at 20 °C, $c_\nu = 0.11$ m/s for the relaxation of oxygen and $c_\nu = 0.0217$ m/s for the relaxation of nitrogen [Pierce,

1981], [Blackstock, 2000]. In the Martian atmosphere at 26 °C, $c_\nu = 10.40$ m/s for the relaxation of carbon dioxide. Because of the sum term included in Equation 5.1, it can only be solved numerically. A code developed at the University of Texas by Cleveland, Hamilton, and Blackstock was used for solving the augmented Burgers Equation.

5.2 Numerical Burgers' Solver

Cleveland, Hamilton, and Blackstock built a Fortran numerical solver that is used for "time-domain modeling of finite-amplitude sound in relaxing fluids" [1996]. It is capable of of accounting for nonlinear, thermoviscous, and relaxation effects, and an inhomogeneous medium. Up to five relaxation effects can be input. It will model plane, cylindrical and spherical propagations. The code is based on a nondimensionalized form of Equation 5.1.

$$\frac{\partial P}{\partial \sigma} = P\frac{\partial P}{\partial t'} + \frac{1}{\Gamma}\frac{\partial P^2}{\partial t'^2} + \sum_\nu D_\nu \int_{-\infty}^{t'} \frac{\partial^2 P}{\partial t''^2} e^{-(t'-t'')/\theta_\nu} dt'' \tag{5.2}$$

$\Gamma = 1/\alpha_0^{tv}\bar{x}$ is the the Gol'berg number, α_0^{tv} is the thermoviscous absorption coefficient, $\bar{x}$ is the shock formation distance, $D_\nu = \rho_0 c_0 c'_\nu/\beta p_0$, is the ratio of absorption to nonlinearity in a different formulation, $\theta_\nu = \omega_0 t_\nu$ is the nondimensionalized relaxation time, $t' = \omega_0\tau$ is the nondimensionalized retarded time, $\sigma = x/\bar{x}$ is the nondimensionalized distance, and $P = p/p_0$ is the nondimensionalized pressure with p_0 being a reference pressure and ω_0 being a reference frequency. For a plane wave, the shock formation distance is $\bar{x} = \rho_0 c_0^3/\beta\omega_0 p_0$. The relaxation time and ratio of absorption to nonlinearity are the main components used to describe the atmosphere the wave propagates through for this code when considering homoegeneous atmospheres.

The code takes an input file that describes the waveform at the source, or can generate a sinusoidal waveform. It outputs an array of waveforms as pressure versus retarded time at values of σ that are chosen upon input.

5.2.1 Code Verification

Provided with the code were text files that list the parameters used by Cleveland et al. to create the plots published in their paper on the solver. Recreating these plots was the first step in verifying the the code functioned and produces expected results. Figure 1 from Cleveland et al., shows comparisons of the numerical results of the solver

with the initial waveform, the multi-valued solution, and with weak shock theory. It shows the same behavior as was found for Mars in the previous chapter.

The next verification of the code was to compute waveforms of a sinusoid at a handful of distances from the source to compare to Cleveland's Figure 2. The top left hand plot of Figure 5.1 shows the results of this calculation. Once it was verified that the code would run these simple scenarios correctly, the parameters were changed to simulate the Earth and Mars. A sinusoid with an a reference frequency, ω_0, was used for all calculations shown in Figure 5.1. Each column of Figure 5.1 has the same ratio of absorption to nonlinearity, and each row has the same relaxation time. The plot in the center of the figure is the representation of Earth with the relaxation processes of nitrogen and oxygen. The bottom right hand corner plot is the representation of Mars with the relaxation process of carbon dioxide. The rest of the plots show how relaxation time and the ratio of absorption to nonlinearity affect the behavior of the waveforms at different distances. For example from the top right hand corner plot of Figure 5.1, if the relaxation time for carbon dioxide was significantly larger, a large amplitude waveform would not form into a sawtooth form, but the nonlinearity would still create the peak shift behavior that leads to shocks. Instead what is seen in the bottom right hand corner of the figure, for this scenario a sinusoid on Mars would have minimal decrease in peak amplitude even at a great distance, though a shock still has not quite formed. This is because the ratio of absorption to nonlinearity is very high for this example.

Because the code requires nondimensional parameters, the relaxation time and the retarded time are always multiplied by a reference frequency even though for an actual blast, there would not be a single frequency. This is a scaling that is undone once the output of the solver is scaled to have dimesions again. The results from Chapter 4 were replicated with the numerical solver as another check that the code worked. Figure 5.2 shows the results of this verification. A peak pressure amplitude of 20 Pa was chosen for Mars for both a sinusoid and a shock front for this comparison. The impedance difference from Earth to Mars discussed in Chapter 2 is how the equivalent peak pressure was determined for Earth.

The bottom right hand corner plot of Figure 5.2 is the replication of Figure 4.1. The length in time and behavior of the deformation of the wavefront matches in these plots which provides confidence that the code can accurately compute high amplitude wave propagation with Martian parameters. With confirmation that the solver can simulate nonlinear wave propagation on Mars, a model of a realistic meteor blast is needed to be the input for the solver.

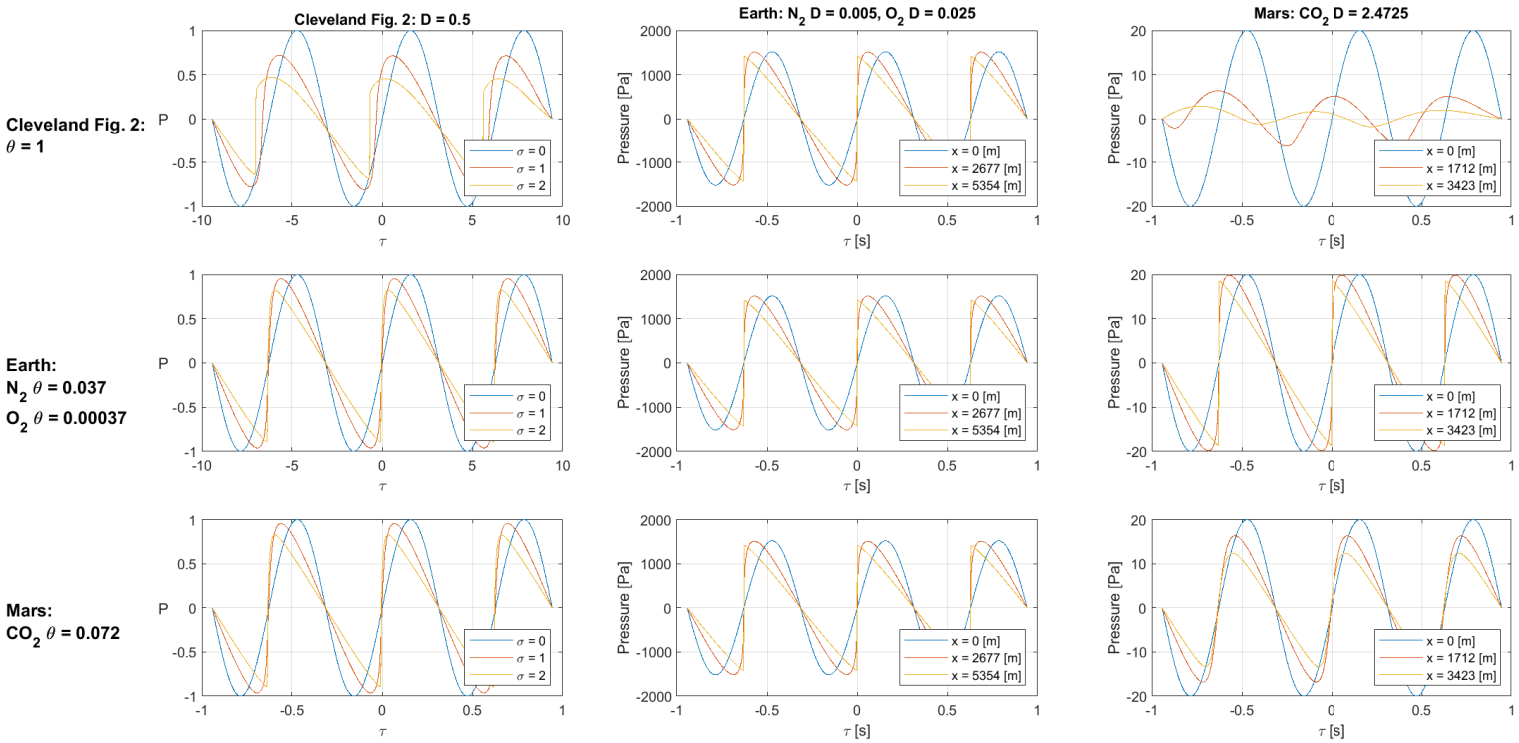

Figure 5.1: Calculation matrix of sinusoidal waves with a reference frequency of $\omega_0 = 10$, for different relaxation values. τ is retarded time, θ is the nondimensionalized relaxation time, and D is the ratio of absorption to nonlinearity for a fluid.

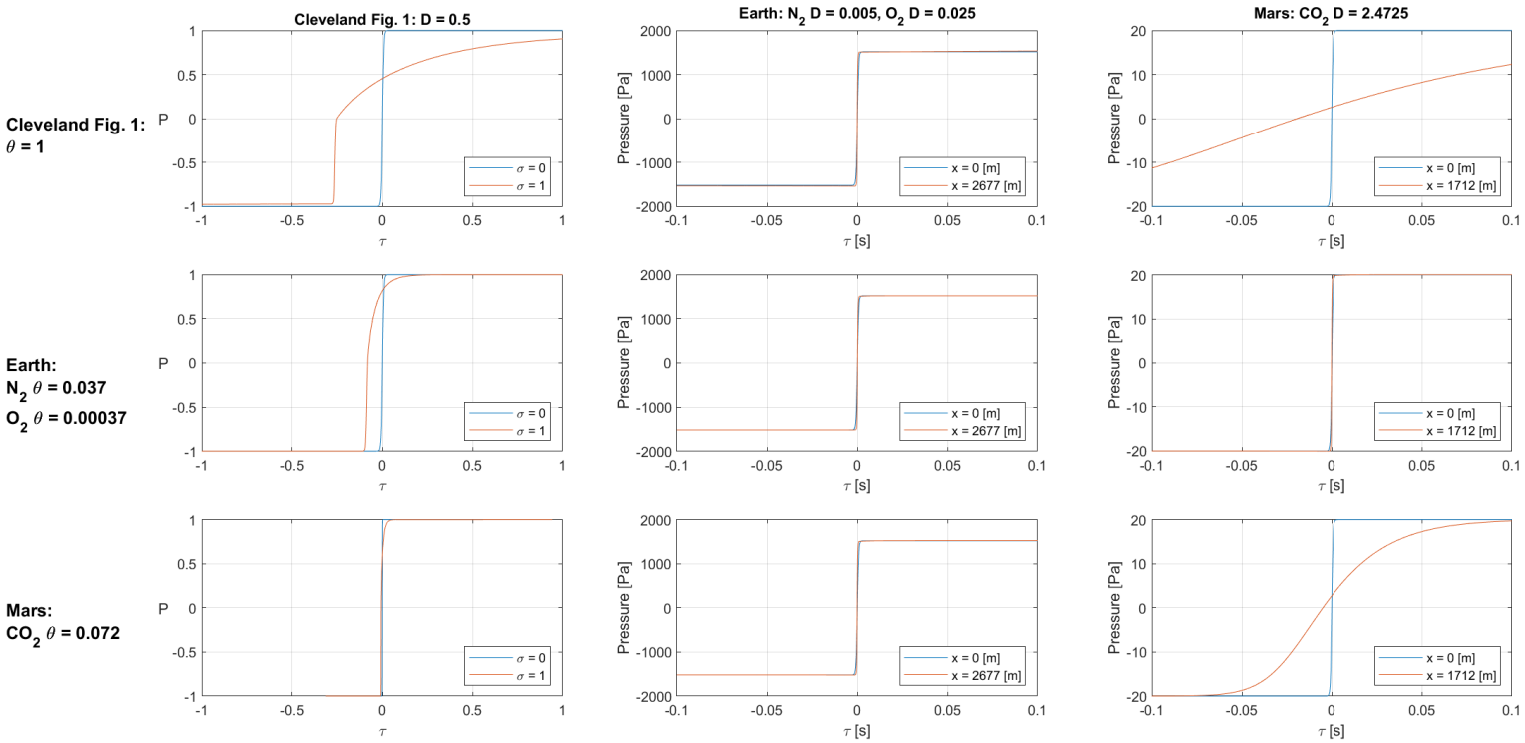

Figure 5.2: Calculation matrix of a step function pressure jump with a reference frequency of $\omega_0 = 10$, for different relaxation values. τ is retarded time, θ is the nondimensionalized relaxation time, and D is the ratio of absorption to nonlinearity for a fluid.

5.3 A Realistic Meteor Blast Pulse Model

The blast pulse predicted by Nemec et al. shown in Figure 1.3 was used as basis for creating the initial blast pulse. An ideal blast, based on work from Sparrow and Raspet was used as the initial input to the Cleveland Burgers' solver. This pulse uses the ratio of $\Delta p/p_\infty$ of meteor 20090428 from Nemec et al., nearly one half, to create a blast pulse that would have an accurate amplitude in the Martian atmosphere. p_∞ is the ambient atmospheric pressure. On Mars near the surface it is in the range of 600 Pa, so the peak pressure of the pulse is around 300 Pa. Figure 5.3 shows the blast pulse used as the initial waveform input for the Burgers' solver. This plot is scaled by a reference pressure equal to the peak pressure so as to be nondimensionalized for use with the solver. All outputs are multiplied by the reference pressure to get accurate pressure amplitudes.

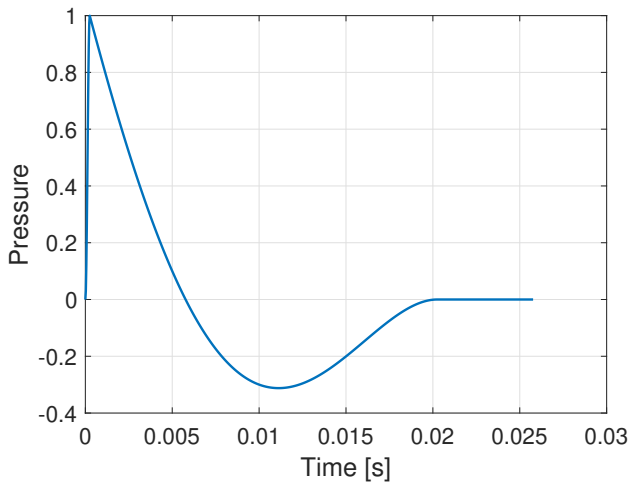

Figure 5.3: Initial blast pulse in the nearfield of a meteor passing through the Martian atmosphere. The pressure has been scaled by a reference pressure to make it nondimensional.

5.4 Results

The trajectory of the meteor considered in the calculations presented below is perpendicular to the ground surface, such that sound rays would be travelling parallel to the ground. Since the calculations use a homogeneous atmosphere, the meteor as a source is considered to be at a low altitude.

5.4.1 Propagation through Earth's atmosphere

The first calculations were done using the Earth's atmosphere, to assess if the results are realistic. The propagation distance from Meteor 20090428 to the IMS receiver was greater than 100 km [Nemec et al., 2017]. For this check, shorter distances were evaluated to analyze the changing wave behavior. Figures 5.4 and 5.5 show the comparison of the blast pulse modeled as a plane wave and as a cylindrical wave. It is clear that at any distance, the cylindrical spreading greatly changes the amplitude and waveform. Modeling the meteor as a cylindrical source is necessary for accurate predictions of wave propagations. $\sigma = 20$ corresponds to 51.8 m, and $\sigma = 200$ corresponds to 518.1 m from the source on Earth, where σ is the distance, x, from the source that the waveform is recorded at, divided by the shock formation distance, $\bar{x}$.

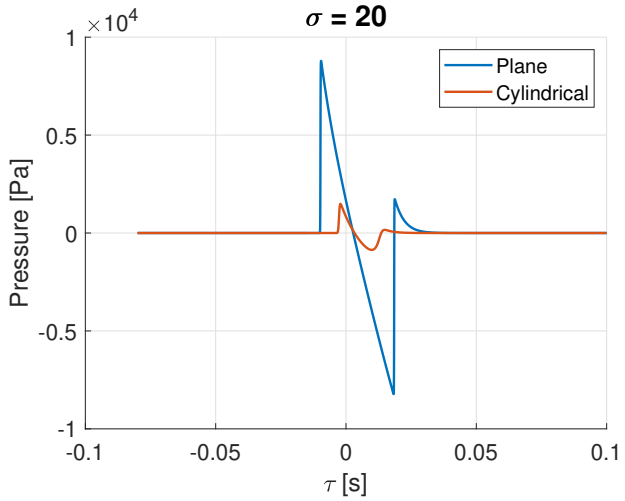

Figure 5.4: Meteor blast wave propagated through Earth's atmosphere to $\sigma = 20$ or 51.8 m as a plane wave and as a cylindrical wave. σ is the nondimensional distance from the source.

A comparison of the sound pressure level for this model confirms the need to use the augmented Burgers Equation to model the meteor blast. Figure 5.6 shows the sound

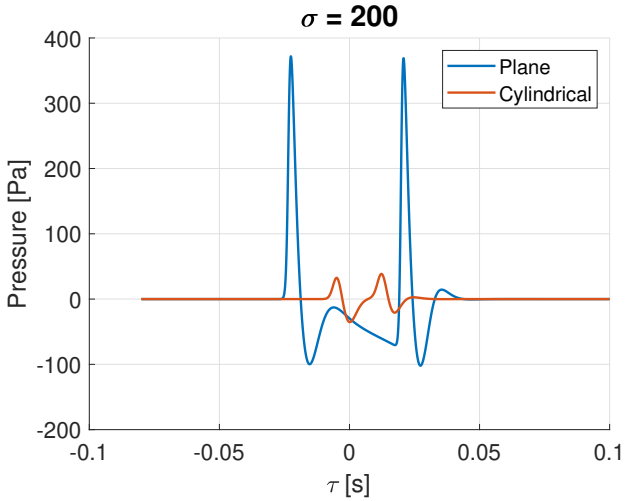

Figure 5.5: Meteor blast wave propagated through Earth's atmosphere to $\sigma = 200$ or 518.1 m as a plane wave and as a cylindrical wave. σ is the nondimensional distance from the source.

pressure level prediction of a meteor blast wave using only linear acoustic theory with cylindrical spreading, the same theory with the absorption coefficient for a frequency of 4000 Hz, an the sound pressure level at each range point output from the Burgers' solver. The nonlinear model agrees well with the linear model with absorption for distances close to the source, but at larger distances, the linear absorption model predicts a steady decrease in sound level. The nonlinear model includes the energy transfer from the fundamental frequencies of the wave into the harmonics, which keeps the sound level from decaying as fast as a linear sound. With the high pressure amplitude and the energy redistribution during propagation, blast waves travel extremely far distances on Earth, especially the low frequency content because it is absorbed less by the atmosphere. The expectation is that the same is true for Mars, despite the atmosphere being more absorbent overall.

5.4.2 Propagation through the Martian atmosphere

The ambient pressure of the Martian atmosphere near the the surface is 636 Pa. The peak pressure amplitude for the blast pulse on Mars was determined by using the peak from Figure 1.3 with 636 Pa as p_∞. The blast pulse in Figure 5.3 was used with the new pressure amplitude and the absorption processes of Mars for a number of distances to analyze the waveform transformation and the sound pressure level. Figure 5.7 shows the waveform at $\sigma = 10$ or 34.2 m and $\sigma = 20$ or 68.5 m from the source on Mars.

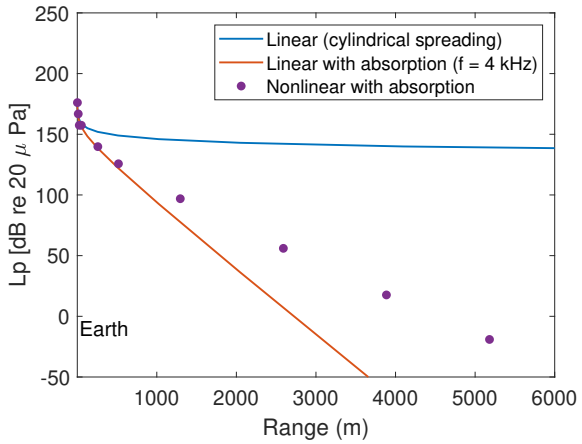

Figure 5.6: Comparison of the sound pressure level using three acoustic models of meteor blast wave propagation on Earth: linear propagation with cylindrical spreading attenuation (blue), linear propagation with cylindrical spreading attenuation and atmospheric absorption (orange), nonlinear propagation with cylindrical spreading attenuation and atmospheric absorption (purple).

The immediate observation from Figure 5.7 is that the shape of the waveform is much smoother spread over time than for the same blast wave on Earth at a much farther distance. This confirms what the previous chapters discussed about the absorption and the effect it has on sound propagation on Mars. Having a pressure change to ambient pressure ratio near 0.5 is very high though, and the pressure amplitude for Mars is still very large at almost 70 m away from the source.

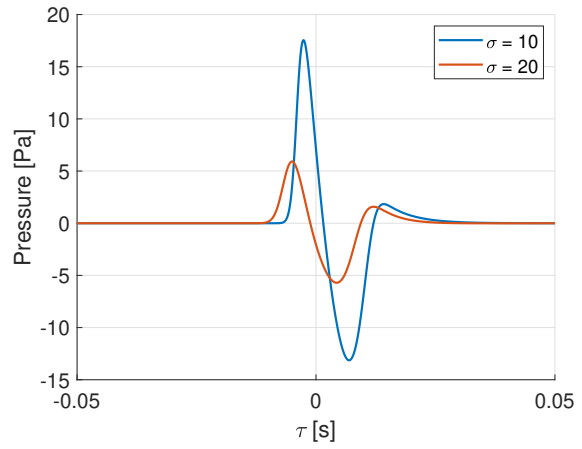

Figure 5.7: Meteor blast wave propagated through the Martian atmosphere to $\sigma = 10$ or 34.2 m and $\sigma = 20$ or 68.5 m. σ is the nondimensional distance from the source.

In Chapter 3, the sound pressure level for sinusoidal plane waves on Mars was modeled considering only the sound absorption. A comparison of sound pressure level for three models of acoustics on Mars for the blast wave shows how the simplified case for a plane wave tells an incomplete story of sound propagation on Mars. Figure 5.8 shows the sound pressure level prediction of a meteor blast wave using only linear acoustic theory with cylindrical spreading, the same theory with the absorption coefficient for a frequency of 100 Hz, an the sound pressure level at each range point output from the Burgers' solver. It is expected that linear acoustic theory without absorption predicts levels that are far too high. The comparison of linear acoustic propagation with absorption to nonlinear acoustic propagation shows that the absorption on Mars only significantly reduces propagation distance for sounds that behave linearly. Based on the results presented here, meteor blast waves should travel hundreds of meters farther from the source than linear acoustic calculations predict. With the likelihood of more meteoroids passing through the Martian atmosphere in the future, there will be opportunities to record sonic blast waves.

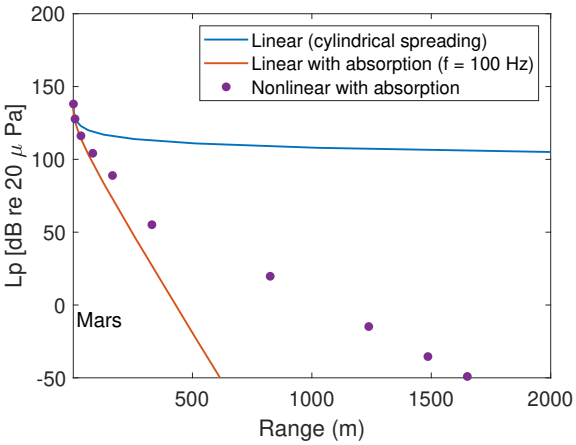

Figure 5.8: Comparison of the sound pressure level using three acoustic models of meteor blast wave propagation on Mars: linear propagation with cylindrical spreading attenuation (blue), linear propagation with cylindrical spreading attenuation and atmospheric absorption (orange), nonlinear propagation with cylindrical spreading attenuation and atmospheric absorption (purple).

5.5 Summary

An augmented Burgers Equation solver can be used to model meteor blast waves on Mars. Cylindrical spreading needs to be taken into account for accurate waveform predictions, but despite the high atmospheric absorption and the attention from cylindrical spreading, sound from a meteor should travel great distances on Mars. The next section discusses how this work could be improved upon and what applications it has to the study and exploration of Mars.

Chapter 6
Conclusion

The goal of this thesis was to apply nonlinear acoustic theory to show that meteor blast waves will propagate significant distances on Mars. Models of the atmosphere suggest that due to the molecular relaxation of carbon dioxide at the temperatures and density found on Mars, sound at all frequencies will be more absorbed by the Martian atmosphere than Earth's. With high amplitude sounds, a nonlinear wave equation is used to predict sound propagation. These sounds generally travel longer distances because energy is stored in the wave longer. Since there have been recent documented meteorite impacts on Mars, a meteor blast is a realistic high amplitude source to be found in the Martian atmosphere. It was shown that in both analytical and numerical models, nonlinearity will not be completely dominated by the high absorption from the atmosphere, even when considering cylindrical wave attenuation. The sharp N-waves heard as two consecutive booms on Earth are not expected to appear as such on Mars, but the collection of infrasound data from meteor blasts can be utilized. Infrasound sensing would aid in distinguishing seismic activity from meteorite impacts as the sound data can be correlated with seismic and visual data. This is useful in the goal of understanding the evolution of Martian geological systems. Infrasound sensing is also a tool that can be applied to human exploration missions for safety and study of human wellness. Knowing what sounds will be heard by humans on Mars, especially low frequencies that can travel through spacesuits, will inform training for psychological preparedness.

6.1 Future Work

Continuation of this work would include increasing the complexity of the model of the Martian atmosphere and of the meteor blast to make each more realistic. To improve the model of the Martian atmosphere, an inhomogeneous atmospheric profile could be

implemented. The Burgers' solver used for this work allows for an inhomogeneous atmosphere, as do other numerical solvers. This profile would add wind, a temperature gradient with altitude, and possibly a density gradient with altitude. The atmosphere was modeled as pure carbon dioxide, but the solver used allows for up to five relaxation processes. More accurate models could include the relaxation process of other gases in the Martian atmosphere. Reflections from the ground were not included in any models discussed. Mars does not have have the same amount of variety in ground surfaces as Earth, and a simple model of the ground could be included to determine if ground reflections would have an impact on the propagation of meteor blast waves.

A further analysis of the blast wave could be done in the future. Creating a blast wave that better matches those that have been predicted on Earth would improve the accuracy of propagation predictions. With more time, more analysis of the waveform transformation at even longer distances would allow for better comparison to examples from meteors on Earth.

Appendix A
MATLAB code for Bass and Chambers Absorption Model

Below is the MATLAB code written to recreate the plots from Bass and Chambers. All values are pulled from the Mars fact sheet [NASA, 2024], Sutherland and Bass, or Bass and Chambers. What is shown is for the absorption coefficients at a temperature of 300 K. Changing the T variable at the beginning to 200 K will produce the other plot from the paper.

A.1 MATLAB Code

```
%% Absorption Equations for Mars Atmosphere
clear variables
close all
clc

% Temp range: 140K - 300K
T = 300; % K

% frequency range:
f = (1:1:10000)'; % frequency in Hz
w = 2*pi.*f; % omega

% mean molecular weight
M = 43.34; % kg/kmol

% gas constant
```

```
17 R = 8.31432E3; % J/kmol/K
18
19 % atmospheric pressure
20 P = 636; % N/m^2 - 6.36 mbar
21
22 % equilibrium density
23 p0 = 0.020; % kg/m^3
24
25 %% Classical Absorption:
26
27 % beta and S are emperical values for CO2
28 beta = 1.49E-6; % kg/m/sqrt(K)/s, Sutherland Equation
29 S = 217; % K
30
31 % viscosity, mu [kg/m]
32 mu = beta*T^(1/2)/(1+(S/T));
33
34 % Characterisitic Temperature of a vibrational mode for CO2 [K]
35 thetaj = 960;
36
37 % Cv/R for the PlankEinstein relation
38 CvR = 3/2 + 0.98 +(2*0.95*(960/T)^2*exp(-960/T))/(1-exp(-960/T))^2; % ...
       Cv/R with Cj'/R
39
40 % Specific heat a constant volume [J (kg kmol)^-1 K^-1]
41 Cv = CvR*R;
42
43 % ratio of specific heats
44 gamma = (CvR+1)/CvR;
45
46 % speed of sound [m/s]
47 c0 = sqrt(gamma*R*T/M);
48
49 % Classical Absoprtion coeffiecient (Np/m)
50 alphacl = ...
       (2*pi^2*f.^2/(gamma*P*c0))*mu*(4/3+((gamma-1)/gamma)*(15/4)*(4/15+3*R/5/Cv));
51
52 %% Rotational Relaxation Absorption
53
54 %rotational collision number
55 Zrot = 61.1*exp(-16.8/(T^(1/3)));
56
```

```
% specific heat ratio excluding vibrational contribution
gammaex = 7/5;

% speed of sound with new gamma
cinf = sqrt(gammaex*R*T/M);

% specific heat at constant pressue for low freq, above relaxation freq
Cp0 = 7/2*R;

% rotational absorption coefficient (Np/m)
alpharot = ...
    (2*pi^2*f.^2/(gammaex*P*cinf))*mu*(gammaex*(gammaex-1)*R/(1.25*Cp0))*Zrot;

%% Vibrational Absorption

% specific heats at frequency well above the relaxation frequency of CO2
Cvinf = 3*R;
Cpinf = Cvinf+R;

% rate of energy transfer from CO2 during collision with itself, N2, Ar,
% and H2O
kCO2 = 0.219*P/mu*exp(-60.75/T^(1/3));
kN2 = 1.44*P/mu*exp(-78.29/T^(1/3));
kAr = kN2;
kH2O = 6e-2*1.25*P;

% mole fraction of each component
XCO2 = 0.95;
XN2 = 0;%0.027;
XAr = 0;%0.016;
XH2O = 0;%0.021;

k = XCO2*kCO2+XN2*kN2+XAr*kAr+XH2O*kH2O; % [1/s] rate at which CO2(v2) ...
    transfers vibrational energy (forward reaction rate)
kb = k*exp(-thetaj/T); % reverse reaction rate
tau_vT = 1/(k-kb); % relaxation time at constant volume and temparture
tau_vs = (Cpinf/Cp0)*tau_vT; % relaxation time for a single energy ...
    transfer

% relaxation frequency
fr = 1/(2*pi*tau_vs);
%fr = 240;
```

```
96
97  % Cj'/R for the PlankEinstein relation
98  CjR = (2*0.95*(thetaj/T)^2*exp(-thetaj/T))/(1-exp(-thetaj/T))^2;
99
100 % relaxation strength
101 s = CjR*R^2/(Cpinf*(Cvinf+CjR*R));
102
103 % vibrational relaxtion absorption coefficient (Np/m)
104 alphavib = (pi*s/cinf)*(f.^2/fr)./(1+(f/fr).^2);
105
106 % Total Absorption
107 alpha_tot = alphacl + alpharot + alphavib;
108
109 %% save absorptions
110 %  output_filename = ['C:\Users\lrh5483\OneDrive - The Pennsylvania ...
       State University\Documents\MATLAB\Mars Absorp' 'alphamars'];
111 %  save(output_filename, 'alphavib', 'alpharot', 'alphacl' );
112 %
113 % output_filename = ['C:\Users\Lily\Documents\MATLAB\Mars\Mars ...
       Absorp\' 'mars_T300K'];
114 % save(output_filename, 'alpha_tot', 'gamma', 'gammaex', 'Cpinf', ...
       'Cp0', 'Cv', 'Cvinf', 'tau_vs', 'c0', 'cinf', 'p0', 'fr');
115
116 %% Graphing absoprtion coefficient
117
118 figure(1)
119 ax = gca;
120 loglog(f,alpharot, 'LineWidth', 2)
121 hold on
122 loglog(f,alphavib, 'LineWidth', 2)
123 loglog(f,alphacl, 'LineWidth', 2)
124 loglog(f, alpha_tot,'--', 'LineWidth', 2)
125 grid on
126 legend('Rotational', 'Vibrational', 'Classical', 'Total')
127 xlabel('Frequency [Hz]')
128 ylabel('Absorption [Np/m]')
129 title('Absorption coefficients of Mars')
130 plftsz(14, 16, 16, 18);
```

Appendix B
MATLAB code for the analytical solution for Burgers' Equation

The code shown below uses parameters for the Martian atmosphere (ratio of specific heats, sound speed etc.) at 300 K. It is broken into three sections: solving for the pressure of a wave front for $D > 1$, $D = 1$, and $D \leq 1$. For the $D \leq 1$, the fzero function was used. It uses a collection of algorithms to find the zeros of a nonlinear equation. See MATLAB help for more information on fzero.

B.1 MATLAB Code

```
%% Non-linear Mars
clear variables
close all
clc

%load in parameters of Martian atmosphere
mars = load('mars_T300K.mat');
gamma_0 = mars.gamma;       % ratio of specific heat below relax freq
gamma_inf = mars.gammaex;   % ratio of specific heat above relax freq
c0 = mars.c0;               % speed of sound below molecular relaxtion ...
    freq
cinf = mars.cinf;           % speed of sound above mo relx freq
Cp0 = mars.Cp0;             % specific heat at constant below
Cpinf = mars.Cpinf;         % specific heat at constant above
rho0 = mars.p0;             % atmospheric pressure of mars at surface
fr = mars.fr;               % relaxation frequency of mars atm
```

```
16 alpha = mars.alpha_tot;     % total atm absorption
17
18 % time vector
19 t = -0.1:.001:0.1; % [s]
20
21 % frequency vector
22 f = (1:1:1000)'; % [Hz]
23 omega = 2*pi*f;
24
25 % distance
26 x = 0;
27
28 % retarded time [s]
29 tau = t-x/c0;
30
31 %% At temperature T = 300 K
32
33 tr = 1/fr; % relaxation time
34
35 % coefficient of nonlinearity (below relaxation frequency)
36 beta_0 = (gamma_0+1)/2;
37
38 % coefficient of nonlinearity (above relaxation frequency)
39 beta_inf = (gamma_inf+1)/2;
40
41 % Disperion parameter
42 m = (cinf^2-c0^2)/c0^2;
43
44 %% Calculation of waveform for D > 1
45 % Propagation pressure
46 p0 = 1:250; % pressure amplitude [Pa]
47 ndx = length(p0);
48
49 % pre-allocate D and pressure vectors
50 D = zeros(ndx, 1);
51 p = zeros(ndx, length(tau));
52
53
54 %calculate pressure
55 for n = 1:ndx
56
57 % ratio of relaxation effects to nonlinear effects
```

```
D(n, :) = m*rho0*c0^2/2/beta_0/p0(n);

% pressure for D >> 1
p(n, :) = p0(n)*tanh(tau/2./D(n)/tr);

end

p_more_D1 = p(20,:);

%% Calculation of waveform for D = 1

% D = 1 at pressure amplitude 50 [Pa] for T = 300K
D1 = 1;

% retarded arrival time of the shock
tau_sh = -tr*log(4*D1^(1+D1)*(1-D1)^(1-D1));

% tau vector from tau, shock(tsh)
tsh = tau_sh:.001:0.1; % [s]
tauD1 = tsh-x/c0;
% tau start to tau, shock(tsh)
tau0 = -0.1:0.001:tau_sh;
tau_length = length(tau0);
pstart = zeros(tau_length,1)-50;

% pressure amplitude for D = 1
p0_D1 = p0(:,50);
pD1 = p0_D1*(1-exp(-tauD1/2/tr));

% combine pressure start and pressure shock
pD1 = [pstart; pD1'];
tauD1 = [tau0'; tauD1'];

%% Calculation of waveform for D < 1

% D_less_1 = D(51:end,:);
% dex = length(D_less_1);

D05 = 0.5; %D(100,:); % D = 0.5 roughly
p05 = p0(:,100);


```

```
% tau vector
tau_D05_start = -0.1:0.001:0; % tau_shock = 0 for D = 0.5
tau_D05 = 0:0.001:0.006;
tau_D05_length = length(tau_D05_start);

% first interation of searching for the zeros of the nonlinear eq
for idx = 1:length(tau_D05)

% find when tau - ln(p/p) is zero
myfun = @(p, tau_f) tau_f - tr*log(((1+p/p05).^(D05-1))./((1-p/p05) ...
    .^(D05+1)));
tau_f = tau_D05(idx);

fun = @(p) myfun(p, tau_f);
pD05(idx,:) = fzero(fun, [-17 50]);

end

%step in time
tau_D06 = 0.006:0.001:.047;
tau_D06_length = length(tau_D06);

% second interation of searching for the zeros of the nonlinear eq
for idx = 1:length(tau_D06)

% find when tau - ln(p/p) is zero
myfun = @(p, tau_f) tau_f - tr*log(((1+p/p05).^(D05-1))./((1-p/p05) ...
    .^(D05+1)));
tau_f = tau_D06(idx);

fun = @(p) myfun(p, tau_f);
pD06(idx,:) = fzero(fun, [20 99]);

end

%step in time
tau_D07 = 0.048:0.001:0.1;
tau_D07_length = length(tau_D07);

% third interation of searching for the zeros of the nonlinear eq
for idx = 1:length(tau_D07)

```

```
% find when tau - ln(p/p) is zero
myfun = @(p, tau_f) tau_f - tr*log(((1+p/p05).^(D05-1))./((1-p/p05) ...
    .^(D05+1)));
tau_f = tau_D07(idx);

fun = @(p) myfun(p, tau_f);
pD07(idx,:) = fzero(fun, [80 99.9999]);

end

% add pressure at tau before tau_shock
pD05start = zeros(tau_D05_length,1)-p05;

%build pressure vector from nonlinear zeros searches
pD051 = [pD05start; pD05; pD06; pD07];
tau_D051 = [tau_D05_start tau_D05 tau_D06 tau_D07];



%% Rise Time (only works if x = 0, otherwise must create time vector)
    % using tau vectors to find rise time with Tau = t - x/c, where x ...
       = 0.

% D >> 1
p1 = 20 + p_more_D1;
p1_10 = 0.1*(max(p1));
p1_90 = 0.9*(max(p1));
t11 = find(p1 < p1_10);
t12 = find(p1 > p1_90);
tr1 = tau(min(t12)) - tau(max(t11)); % rise time [s]
lsh1 = c0*tr1;                       % shock thickness [m]


% D = 1
p2 = 50 + pD1;
p2_10 = 0.1*(max(p2));
p2_90 = 0.9*(max(p2));
t21 = find(p2 < p2_10);
t22 = find(p2 > p2_90);
tr2 = tau(min(t22)) - tau(max(t21)); % rise time [s]
lsh2 = c0*tr2;                       % shock thickness [m]

```

```
% D < 1
p3 = 100 + pD051;
p3_10 = 0.1*(max(p3));
p3_90 = 0.9*(max(p3));
t31 = find(p3 < p3_10);
t32 = find(p3 > p3_90);
tr3 = tau(min(t32)) - tau(max(t31)); % rise time [s]
lsh3 = c0*tr3;                       % shock thickness [m]

rise_times = [tr1; tr2; tr3];
D_table = [2.5; 1; 0.5];
shock_thick = [lsh1; lsh2; lsh3];
%% figures

% D > 1
figure(1)
plot(tau, p_more_D1, 'LineWidth', 2)
xlabel('\tau [s]')
ylabel('Pressure [Pa]')
xlim([-0.1 0.1])
ylim([-30 30])
plftsz(18, 20, 20, 22);
title('Pressure wavefront for D = 2.5')
txt1 = {'shock thickness [m]: ',  num2str(lsh1, '%.2f') };
text(0.02, 1, txt1);

% D = 1
figure(2)
plot(tauD1, pD1, 'LineWidth', 2)
xlabel('\tau [s]')
ylabel('Pressure [Pa]')
xlim([-0.1 0.1])
ylim([-60 60])
plftsz(18, 20, 20, 22);
title('Pressure wavefront for D = 1')
txt2 = {'shock thickness [m]: ',  num2str(lsh2, '%.2f') };
text(0.02, 1, txt2);


% D < 1
figure(3)
plot(tau_D051, pD051, 'LineWidth', 2)
```

```
225 xlabel('\tau [s]')
226 ylabel('Pressure [Pa]')
227 xlim([-0.1 0.1])
228 ylim([-110 110])
229 plftsz(18, 20, 20, 22);
230 title('Pressure wavefront for D = 0.5')
231 txt3 = {'shock thickness [m]: ',  num2str(lsh3, '%.2f') };
232 text(0.02, 1, txt3);
233
234 % Nonlinear acoustics on Mars
235 Weak_Shock = table( D_table, rise_times, shock_thick );
```

Appendix C
Code for the numerical Burgers' solver and meteor blast calculations

C.1 BurgersTX Code

This section contains the input parameters used in the BurgersTX Fortran code developed at the University of Texas, Austin by Cleveland et al.. These are the parameter inputs used to simulate Earth's atmosphere and Mars' atmosphere as discussed in Chapter 5. Also included in this appendix is the code to create the initial blast pulse "int_blast.txt" file used as the input waveform and the code to create the acoustic model comparison plots in Figure 5.6 and Figure 5.8.

Microsoft Visual Studio was used with the Intel Fortran Compiler to compile the BurgersTX code and produce the executable file for the solver. The compiler is invoked using the command "ifx" followed by the "BurgersTX.f" file to be compiled. Once the executable file is made, it is run in the command prompt window. When the solver is started it will ask for a number of parameters including choosing to include or exclude nonlinear effects, thermoviscous effects, and so on. The following input parameters follow the order and form in which the file requests the inputs. One and zero are yes and no for prompts such as nonlinear effects. the file "int_blast.txt" is plain text taken from the output of the initial blast pulse generated with the MATLAB code shown in Appendix C.3.

C.1.1 Input parameters for a meteor blast on Earth

```
1 #nonlinear effects
1 #thermoviscous effects
1 #relaxation effects
0 #inhomogeneous medium flag
0 #spreading (0:plane, 0.5:cylindrical, 1.0:spherical)
1 #Calculate (0) or load (1) waveform
int_blast.txt
1   #num cycles in wave
0 #num cycles before wave
1 #num cycles after wave
0   #num points (cuurently ignored for loaded waveforms)
0.001 #TV
2 #numRelax
0.00015 1.2566 #D theta
0.00080 0.015 #D theta
0.1 #start sigma
11 #num output locations
1
5
10
20
100
200
500
1000
1500
2000
2001
0.0012 #stepsize
```

C.1.2 Input parameters for a meteor blast on Mars

```
1 #nonlinear effects
1 #thermoviscous effects
```

```
1 #relaxation effects
0 #inhomogeneous medium flag
0.5 #spreading (0:plane, 0.5:cylindrical, 1.0:spherical)
1 #Calculate (0) or load (1) waveform
int_blast.txt
1   #num cycles in wave
3 #num cycles before wave
3 #num cycles after wave
0   #num points (cuurently ignored for loaded waveforms)
0.0000015 #TV
1 #numRelax
0.0642 2.2729 #D theta
0.1 #start sigma
11 #num output locations
1
5
20
50
100
250
500
750
900
1000
1001
0.0012 #stepsize
```

C.2 Initial Blast Pulse

```
1 %% Initial Blast Pulse
2 clear variables
3 close all
4 clc
5 %%
```

```
% initial conditions
scale = 500;
Δp0 = 1;            % Pa
tau = (40E-6)*scale;      % seconds
t1 = 0.5E-6*scale;        % seconds
tplus = 11.0326e-6*scale; % seconds
t2 = 0.502930e-6*scale;   % seconds
t3 = 0.505859e-6*scale;   % seconds

% time vecotor
time1 = linspace(0, t3, 10);
time2 = linspace(t3, t2+tau, 1538);
time3 = linspace(t2+tau, t2+tau+tplus, 500);

% pressure calculation
pt1 = Δp0/2*(1-cos(pi.*time1./t1));
pt2 = Δ...
    p0*(1-(time2-t2)./tplus).*(1-(time2-t2)./tau).*(1-((time2-t2)./tau).^2);
pt3 = 0*time3;

%plot
timetot = [time1, time2, time3];
ptot = ([pt1, pt2, pt3])';


figure(1)
plot(timetot, ptot, 'LineWidth', 1.5)
xlabel('Time [s]')
grid on
ylabel('Pressure')
plftsz(14, 16, 16, 18);

%% save vector
output_filename = ['C:\Users\lrh5483\OneDrive - The Pennsylvania State ...
    University\Documents\MATLAB\Numerical\' 'initialblast'];
save(output_filename, 'ptot' );
```

C.3 Meteor Propagation Plots

```
%% Refresh
clear variables
close all
clc

%% load data


NtND = readtable('Earth_D_theta_pulse1.txt');
mars_cyl = readtable('Mars_D_theta_pulse_cyl.txt');

% thermoviscous absoprtion for all: 0.001 np/m
% N2 relaxation frequency, 250 Hz; RH = 30%, T = 20 deg C
% p0 = 20 Pa at 60km

% Earth atmoshpere at 20 deg C
rho_0_E = 1.21; % density of air kg/m^3
c_0_E = 343; % speed of sound m/s
beta_E = 1.2; % coefficient of nonlinearity
cvN = 0.0217; % small-signal sound speed increment, nitogren
cvO = 0.115; % small-signal sound speed increment, oxygen
frN = 250; % relaxation frequency at 30% humidity, 20 deg C for nitorgen
frO = 21000; % relaxation frequency at 30% humidity, 20 deg C for oxygen
alpha_cl = 50^2*1.84e-11*sqrt(293/293.315); % classical abs for Earth ...
    at 20 deg C

% Mars atmosphere at 300 K
mars = load(['C:\Users\Lily\OneDrive - ' ...
    'The Pennsylvania State University\Documents\MATLAB\' ...
    'Mars Absorp\mars_T300K.mat']);
cvCO = 9;
frCO = mars.fr;
rho_0_M = 0.020; % density of atmos kg/m^3
c_0_M = 270; % speed of sound m/s
beta_M = 1.15; % coefficient of nonlinearity


% angular frequnecy
```

```
omega = 100*pi;


% reference pressure/peak pressure
p0_E = 50000; % Pa
p0_M = 636/2; %p0_E/1.21/343*0.02*273.4; % Pa

% Relaxation processes

    % relaxation of nitrogen on Earth
    D_E_N = rho_0_E*c_0_E*cvN/beta_E/p0_E; % D for nitrogen on Earth
    theta_E_N = omega*1/frN;               % Theta for nitrogen on Earth

    % relaxation of oxygen on Earth
    D_E_O = rho_0_E*c_0_E*cvO/beta_E/p0_E; % D for oxygen on Earth
    theta_E_O = omega*1/frO;               % Theta for oxygen on Earth

    % relaxation of carbon dioxide Mars
    D_M_CO = rho_0_M*c_0_M*cvCO/beta_M/p0_M; % D for CO2 on Mars
    theta_M_CO = omega/frCO;                  % Theta for CO2 on Earth

% shock formation distance
% peak source pressure:  Mars 20 Pa, Earth 1520 Pa
% frequency: 1/(2pi) Hz -> angular frequency: 1 s^-1

% shock formation distance for Earth
x_bar_E = shock_f_distance(rho_0_E, c_0_E, beta_E, p0_E, omega);
x_E = [x_bar_E, 60000];
sigma_E = x_E./x_bar_E;

% shock formation distance for Mars
x_bar_M = shock_f_distance(rho_0_M, c_0_M, beta_M, p0_M, omega);
x_M = [x_bar_M, 60000];
sigma_M = x_M./x_bar_M;


%% plot

figure(2)
%plot((mars_cyl.Var1+pi)/omega, mars_cyl.Var2*p0_M,'LineWidth', 1.5)
hold on
%plot((mars_cyl.Var1+pi)/omega, mars_cyl.Var3*p0_M,'LineWidth', 1.5)
```

```
plot((mars_cyl.Var1+pi)/omega, mars_cyl.Var5*p0_M, 'LineWidth', ...
    1.5)%,'Color', [0.9290, 0.6940, 0.1250])
plot((mars_cyl.Var1+pi)/omega, mars_cyl.Var6*p0_M, 'LineWidth', 1.5)
legend('\sigma = 10','\sigma = 20');%, '\sigma = 200')
plftsz(14, 16, 16, 18);
grid on
xlabel('\tau [s]')
ylabel('Pressure [Pa]')
xlim([-0.05 0.05])
```

C.4 Meteor Sound Pressure Level

```
%% Nonlinearity of meteor blast

%% Refresh
clear variables
close all
clc

%% Levels for Earth Meteor

% Earth atmoshpere at 20 deg C
rho_0_E = 1.21; % density of air kg/m^3
c_0_E = 343; % speed of sound m/s
beta_E = 1.2; % coefficient of nonlinearity
cvN = 0.0217; % small-signal sound speed increment, nitogren
cvO = 0.115; % small-signal sound speed increment, oxygen
frN = 250; % relaxation frequency at 30% humidity, 20 deg C for nitorgen
frO = 21000; % relaxation frequency at 30% humidity, 20 deg C for oxygen
alpha_cl = 50^2*1.84e-11*sqrt(293/293.315); % classical abs for Earth ...
    at 20 deg C

% Mars atmosphere at 300 K
rho_0_M = 0.020; % density of atmos kg/m^3
c_0_M = 270; % speed of sound m/s
beta_M = 1.15; % coefficient of nonlinearity

% reference pressure/peak pressure
p0_E = 50000; % Pa
pref = 20*10^-6; % Pa
```

```
28 p0_M = 660; % Pa (658.74)
29
30 % frequency of initial blast
31 omega = 100*pi;
32
33
34 %% Earth
35 % output from BurgersTX
36 cyl_E = readtable('Earth_D_theta_pulse1.txt');
37
38 tau = (cyl_E.Var1+pi)/omega; % time vector from BurgersTX output
39 s1_E = cyl_E.Var2*p0_E; % wave form at sigma = 0
40 s2_E = cyl_E.Var3*p0_E; % wave form at sigma = 1
41 s3_E = cyl_E.Var4*p0_E; % wave form at sigma = 5
42 s4_E = cyl_E.Var5*p0_E; % wave form at sigma = 10
43 s5_E = cyl_E.Var6*p0_E; % wave form at sigma = 20
44 s6_E = cyl_E.Var7*p0_E; % wave form at sigma = 200
45 s7_E = cyl_E.Var8*p0_E; % wave form at sigma = 2000
46
47 ppeak_E = [max(abs(s2_E)); max(abs(s3_E)); max(abs(s4_E)); max(abs(s5_E));
48     max(abs(s6_E)); max(abs(s7_E))]; % peak pressure from each wave form
49 Lp_E = 20*log10(ppeak_E/pref); % sound pressure level with pressure peak
50 sigma = [1; 5; 10; 20; 200; 2000]; % sigma vector
51
52 % cylindrical spreading decay (3 db down)
53 for m = 1:14
54     m_lin(m) = 2^(m-1);
55 end
56
57 % shock formation distance
58 x_bar_E = shock_f_distance(rho_0_E, c_0_E, beta_E, p0_E, omega);
59 x_E = sigma*x_bar_E; % distance from meteor
60 alpha_E = 0.006; % dB/m
61
62 % SPL for linear acoustics models
63 for n = 1:length(m_lin)
64     linear(n) = 20*log10(ppeak_E(1)/pref./sqrt(m_lin(n)));
65     linear_abs(n) = 20*log10(ppeak_E(1)/pref./sqrt(m_lin(n)) ...
66         *exp(-alpha_E*m_lin(n)));
67 end
68
69 %% Mars
```

```
cyl_M = readtable('Mars_D_theta_pulse_cyl1.txt');

tau = (cyl_M.Var1+pi)/omega; % time vector from BurgersTX output
s1_M = cyl_M.Var2*p0_M; % wave form at sigma = 0
s2_M = cyl_M.Var3*p0_M; % wave form at sigma = 1
s3_M = cyl_M.Var4*p0_M; % wave form at sigma = 5
s4_M = cyl_M.Var5*p0_M; % wave form at sigma = 20
s5_M = cyl_M.Var6*p0_M; % wave form at sigma = 50
s6_M = cyl_M.Var7*p0_M; % wave form at sigma = 100
s7_M = cyl_M.Var8*p0_M; % wave form at sigma = 200
s8_M = cyl_M.Var9*p0_M; % wave form at sigma = 500
s9_M = cyl_M.Var10*p0_M; % wave form at sigma = 1000

% peak pressure from each wave form
ppeak_M = [max(abs(s2_M)); max(abs(s3_M)); max(abs(s4_M)); max(abs(s5_M));
    max(abs(s6_M)); max(abs(s7_M)); max(abs(s8_M)); max(abs(s9_M))];
Lp_M = 20*log10(ppeak_M/pref); % sound pressure level with pressure peak
sigmaM = [1; 5; 20; 50; 100; 200; 500; 1000]; % sigma vector

% shock formation distance
x_bar_M = shock_f_distance(rho_0_M, c_0_M, beta_M, p0_M, omega);
x_M = sigmaM*x_bar_M; % distance from meteor
alpha_M = 8.68*0.03; % dB/m

% SPL for linear acoustics models
for n = 1:length(m_lin)
    linearM(n) = 20*log10((ppeak_M(1)/pref./sqrt(m_lin(n))));
    linear_abs_M(n) = ...
        20*log10(ppeak_M(1)/pref./sqrt(m_lin(n)))-alpha_M*m_lin(n);
end
%% plot
figure(1)
plot(m_lin, linear, m_lin, linear_abs, 'LineWidth', 1.3)
hold on
scatter(x_E, Lp_E,'filled', 'LineWidth', 1.3, 'MarkerFaceColor', ...
    [0.4940 0.1840 0.5560])
plftsz(14, 16, 16, 18);
ylim([100 190])
xlim([1 1000])
xlabel('Range (m)')
ylabel ('Lp [dB re 20 \mu Pa]')
legend('Linear (cylindrical spreading)', 'Linear with absorption (f = ...
```

```
    4 kHz)', 'Nonlinear with absorption')
text(30, 110, 'Earth', 'FontSize', 14);


figure(2)
plot(m_lin, linearM, m_lin, linear_abs_M, 'LineWidth', 1.3)
hold on
scatter(x_M, Lp_M, 'filled', 'LineWidth', 1.3, 'MarkerFaceColor', ...
    [0.4940 0.1840 0.5560])
plftsz(14, 16, 16, 18);
ylim([20 160])
xlim([1 1000])
xlabel('Range (m)')
ylabel ('Lp [dB re 20 \mu Pa]')
legend('Linear (cylindrical spreading)', 'Linear with absorption (f = ...
    100 Hz)', 'Nonlinear with absorption')
text(15, 35, 'Mars', 'FontSize', 14);
```

Bibliography

Banfield, D., Spiga, A., Newman, C., Forget, F., Lemmon, M., Lorenz, R., Murdoch, N., Viudez-Moreiras, D., Pla-Garcia, J., Garcia, R. F., Lognonné, P., Özgür Karatekin, Perrin, C., Martire, L., Teanby, N., Hove, B. V., Maki, J. N., Kenda, B., Mueller, N. T., Rodriguez, S., Kawamura, T., McClean, J. B., Stott, A. E., Charalambous, C., Millour, E., Johnson, C. L., Mittelholz, A., Määttänen, A., Lewis, S. R., Clinton, J., Stähler, S. C., Ceylan, S., Giardini, D., Warren, T., Pike, W. T., Daubar, I., Golombek, M., Rolland, L., Widmer-Schnidrig, R., Mimoun, D., Beucler, É., Jacob, A., Lucas, A., Baker, M., Ansan, V., Hurst, K., Mora-Sotomayor, L., Navarro, S., Torres, J., Lepinette, A., Molina, A., Marin-Jimenez, M., Gomez-Elvira, J., Peinado, V., Rodriguez-Manfredi, J.-A., Carcich, B. T., Sackett, S., Russell, C. T., Spohn, T., Smrekar, S. E., and Banerdt, W. B. (2020). The atmosphere of mars as observed by InSight. *Nature Geoscience*, 13(3):190–198.

Bass, H. E. and Chambers, J. P. (2001). Absorption of sound in the martian atmosphere. *Acoustical Society of America Journal*, 109(6):3069–3071.

Bass, H. E., Sutherland, L. C., Zuckerwar, A. J., Blackstock, D. T., and Hester, D. M. (1995). Atmospheric absorption of sound: Further developments. *The Journal of the Acoustical Society of America*, 97(1):680–683.

Begault, D. R. (1994). *3-D Sound for Virtual Reality and Multimedia*. AP Professional.

Blackstock, D. T. (2000). *Fundamentals of Physical Acoustics*. Wiley-Interscience.

Cleveland, R. O., Hamilton, M. F., and Blackstock, D. T. (1996). Time-domain modeling of finite-amplitude sound in relaxing fluids. *The Journal of the Acoustical Society of America*, 99(6):3312–3318.

Edwards, W. N. (2009). Meteor generated infrasound: Theory and observation. In *Infrasound Monitoring for Atmospheric Studies*, pages 361–414. Springer Netherlands.

Garcia, R. F., Daubar, I. J., Beucler, É., Posiolova, L. V., Collins, G. S., Lognonné, P., Rolland, L., Xu, Z., Wójcicka, N., Spiga, A., Fernando, B., Speth, G., Martire, L., Rajšić, A., Miljković, K., Sansom, E. K., Charalambous, C., Ceylan, S., Menina, S., Margerin, L., Lapeyre, R., Neidhart, T., Teanby, N. A., Schmerr, N. C., Banerdt, W. B., Froment, M., Clinton, J. F., Karatekin, O., Stähler, S. C., Dahmen, N. L.,

Durán, C., Horleston, A., Kawamura, T., Plasman, M., Zenhäusern, G., Giardini, D., Panning, M., Malin, M., and Banerdt, W. B. (2022). Newly formed craters on mars located using seismic and acoustic wave data from insight. *Nature Geoscience*, 15:774–780.

Hamilton, M. F. and Blackstock, D. T. (1998). *Nonlinear Acoustics*. Academic Press.

Hanford, A. D. and Long, L. N. (2009). The direct simulation of acoustics on earth, mars, and titan. *The Journal of the Acoustical Society of America*, 125(2):640–650.

Henneton, M., Gainville, O., and Coulouvrat, F. (2015). Numerical simulation of sonic boom from hypersonic meteoroids. *AIAA Journal*, 53(9):2560–2570.

Hetherington, L. and Sparrow, V. (2023). Acoustics on the planet mars: Next steps, including sonic booms. *J. Acoust. Soc. Am.*, 153(3, Pt. 2):A281.

Maurice, S., Chide, B., Murdoch, N., Lorenz, R. D., Mimoun, D., Wiens, R. C., Stott, A., Jacob, X., Bertrand, T., Montmessin, F., Lanza, N. L., Alvarez-Llamas, C., Angel, S. M., Aung, M., Balaram, J., Beyssac, O., Cousin, A., Delory, G., Forni, O., Fouchet, T., Gasnault, O., Grip, H., Hecht, M., Hoffman, J., Laserna, J., Lasue, J., Maki, J., McClean, J., Meslin, P. Y., Le Mouélic, S., Munguira, A., Newman, C. E., Rodríguez Manfredi, J. A., Moros, J., Ollila, A., Pilleri, P., Schröder, S., de la Torre Juárez, M., Tzanetos, T., Stack, K. M., Farley, K., Williford, K., SuperCam Team, Wiens, R. C., Wiens, R. C., Acosta-Maeda, T., Acosta-Maeda, T., Anderson, R. B., Anderson, R. B., Applin, D. M., Arana, G., Bassas-Portus, M., Beal, R., Beck, P., Benzerara, K., Bernard, S., Bernardi, P., Bernardi, P., Bernardi, P., Bosak, T., Bousquet, B., Brown, A., Cadu, A., Caïs, P., Castro, K., Castro, K., Clavé, E., Clegg, S. M., Cloutis, E., Connell, S., Connell, S., Debus, A., Dehouck, E., Delapp, D., Donny, C., Dorresoundiram, A., Dromart, G., Dubois, B., Fabre, C., Fau, A., Fischer, W., Fischer, W., Fischer, W., Francis, R., Frydenvang, J., Gabriel, T., Gabriel, T., Gibbons, E., Gontijo, I., Gontijo, I., Johnson, J. R., Kalucha, H., Kelly, E., Knutsen, E. W., Lacombe, G., Lacombe, G., Lacombe, G., Lacombe, G., Le Mouélic, S., Legett, C., Leveille, R., Lewin, E., Lopez-Reyes, G., Lopez-Reyes, G., Lorigny, E., Madariaga, J. M., Madsen, M., Madsen, S., Mandon, L., Mangold, N., Mann, M., Manrique, J. A., Martinez-Frias, J., Mayhew, L. E., McConnochie, T., McLennan, S. M., Melikechi, N., Melikechi, N., Meunier, F., Meunier, F., Montagnac, G., Montagnac, G., Montagnac, G., Mousset, V., Mousset, V., Nelson, T., Newell, R. T., Newell, R. T., Parot, Y., Parot, Y., Pilorget, C., Pinet, P., Pont, G., Poulet, F., Quantin-Nataf, C., Quertier, B., Rapin, W., Reyes-Newell, A., Robinson, S., Rochas, L., Royer, C., Rull, F., Sautter, V., Sautter, V., Sharma, S., Shridar, V., Sournac, A., Sournac, A., Toplis, M., Torre-Fdez, I., Turenne, N., Turenne, N., Udry, A., Veneranda, M., Venhaus, D., Vogt, D., and Willis, P. (2022). In situ recording of mars soundscape. , 605(7911):653–658.

Mimoun, D., Cadu, A., Murdoch, N., Chide, B., Sournac, A., Parot, Y., Bernardi, P.,

Pilleri, P., Stott, A., Gillier, M., Sridhar, V., Maurice, S., and Wiens, R. (2023). The mars microphone onboard supercam. *Space Science Reviews*, 219(1).

NASA (2018). Insight mission page.

NASA (2024). Mars fact sheet.

NASA/JPL (1999). Mars polar lander mission page.

NASA/JPL (2020). Ingenuity helicopter mission page.

Nemec, M., Aftosmis, M. J., and Brown, P. G. (2017). Computational modeling of meteor-generated ground pressure signatures. In *23rd AIAA/CEAS Aeroacoustics Conference*. American Institute of Aeronautics and Astronautics.

Petculescu, A. (2016). Acoustic properties in the low and middle atmospheres of mars and venus. *The Journal of the Acoustical Society of America*, 140(2):1439–1446.

Petculescu, A. and Lueptow, R. M. (2007). Atmospheric acoustics of titan, mars, venus, and earth. *Icarus*, 186(2):413–419.

Pierce, A. D. (1981). *Acoustics*. McGraw-Hill Book Co.

Sparrow, V. W. (1999). Acoustics on the planet mars: A preview. *The Journal of the Acoustical Society of America*, $106(4_{S}supplement) : 2264 - -2264$.

Sparrow, V. W. and Raspet, R. (1991). A numerical method for general finite amplitude wave propagation in two dimensions and its application to spark pulses. *The Journal of the Acoustical Society of America*, 90(5):2683–2691.

Sutherland, L. C. and Bass, H. E. (2004). Atmospheric absorption in the atmosphere up to 160 km. *The Journal of the Acoustical Society of America*, 115(3):1012–1032.

Williams, J.-P. (2001). Acoustic environment of the martian surface. *Journal of Geophysical Research: Planets*, 106(E3):5033–5041.